

NASA TECHNICAL
REPORT



NASA TR R-163

NASA TR R-163

LOAN COPY:
AFWL (
KIRTLAND A



TECH LIBRARY KAFB, NM
TO
X

HYPERSONIC SHOCK-HEATED FLOW
PARAMETERS FOR VELOCITIES
TO 46,000 FEET PER SECOND AND
ALTITUDES TO 323,000 FEET

by Paul W. Huber

Langley Research Center

Langley Station, Hampton, Va.



HYPERSONIC SHOCK-HEATED FLOW PARAMETERS FOR
VELOCITIES TO 46,000 FEET PER SECOND
AND ALTITUDES TO 323,000 FEET

By Paul W. Huber

Langley Research Center
Langley Station, Hampton, Va.

NATIONAL AERONAUTICS AND SPACE ADMINISTRATION

For sale by the Office of Technical Services, Department of Commerce,
Washington, D.C. 20230 -- Price \$2.00

HYPERSONIC SHOCK-HEATED FLOW PARAMETERS FOR
VELOCITIES TO 46,000 FEET PER SECOND
AND ALTITUDES TO 323,000 FEET

By Paul W. Huber

SUMMARY

Real-air hypersonic-flow parameters are presented in tabular and graphical form for flight in the earth's atmosphere as a function of flight velocity and flight altitude. Thermochemical equilibrium-flow properties are given for the inviscid normal shock and stagnation point, and both equilibrium and frozen-flow parameters, including electron concentration, are listed for the far wake of the inviscid stagnation streamline. Plots of electron collision frequency and electrical conductivity in the normal shock and wake plasmas are also included. The tabulations are made for twelve flight altitudes, ranging from 35,900 feet to 322,900 feet and for flight velocities and shock-heated gas temperatures encompassing those encountered in return from planetary missions. Included are discussions of the applicability of the computed parameters to a given problem, and effects due to the uncertainties in the input data for ambient air.

INTRODUCTION

For many problems in hypersonic aerodynamics, radio communications, and radar tracking which are associated with missions involving flight of bodies at high velocity, the complete distribution of flow-field properties about the vehicle and in the wake must be known. The flight of bodies in the earth's atmosphere at speeds greater than approximately 6,000 feet per second (about 1,800° K) entails a regime of thermodynamics in which the composition of the gas in the region of the body is not fixed at the ambient-air value. This so-called real-gas thermodynamic regime, due to compressive and viscous heating of the gas to high temperature, results in much additional complexity to the flow computation since a wide variety of chemical reactions can occur among the heated species of an air mixture and thus can contribute to the nonideal nature of the thermodynamics and determination of the concentration of important species. However, a number of detailed and comprehensive computational programs have been reported in the literature in which the equilibrium thermodynamic properties of high-temperature air are precisely determined and tabulated. (For example, see refs. 1 to 5.) For the most general application to high-temperature air problems, the above-referenced data,

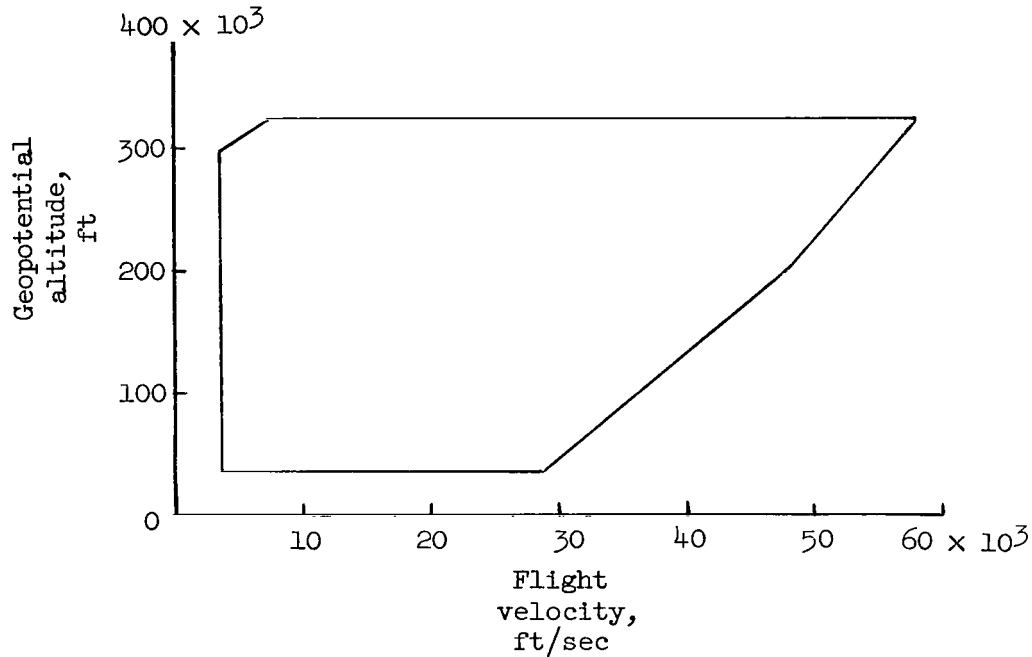
as well as most of such data found in the literature, are tabulated in terms of independent values of two gas-state parameters, usually density ρ and temperature T .

In order then to determine the air-flow properties in the region about a hypersonic body, these real-gas thermodynamic data are used, along with the equations of motion and the conservation equations and iterative solutions are obtained from computer programs. Such procedures are complex and time consuming to program for the complete flow about the body and are applicable only to the particular body shape, velocity, and altitude for which the problem was planned. However, certain portions of the flow fields about hypersonic bodies are independent of the body shape for equilibrium flow and may be characterized in terms of only the flight parameters, velocity and altitude. Such regions include the normal-shock flow, the inviscid stagnation-point flow, the inviscid normal-shock-flow streamline in the far wake, and the oblique-shock flow and corresponding far-wake streamline providing the shock angle is known. "Frozen-flow" far wakes also fall in this category. Tabulation of properties of such real-gas flow regions is generally useful and desirable. For direct applicability to problems involving flight in the earth's atmosphere, it is thus desirable that such tabulation be in terms of independent values of the flight parameters (velocity and altitude) rather than the gas-state parameters ρ and T . This approach avoids the inconvenience of the double interpolation required to apply the density-temperature data to given altitude and velocity conditions, since the earth's atmosphere does involve a specific temperature and density combination. The purpose of the present work is to present such tabulations.

Tabulations and charts were presented in reference 6 for the normal-shock flow properties in terms of flight velocity and altitude for a limited number of altitudes and velocity range. Reference 7 presents tabulated normal-shock parameters and gas composition for many altitudes over a velocity range limited to satellite velocity. Charts for normal and oblique shocks are given in reference 8 for a similar velocity range. Because of the increased emphasis on the higher velocity and higher altitude flights of bodies in missions under current consideration (for example, the return at hyperbolic velocity of vehicles from lunar and planetary missions), the work of references 6 to 8 and others no longer has adequate range for application to many of these problems.¹

¹Subsequent to completion of the computations and final draft of the text that follows, reference 9 became available and is found to contain, in general, the same type of material as the present work. Comparison of the two reports has been made and the following comments are offered: the parameters common to both agree within the accuracy limitations respectively specified, consideration being given to slight differences in altitudes in many cases. As is the case in reference 7, however, the stagnation-temperature computation in reference 9 is made by use of a very approximate method, which results in errors of over 50 percent in the temperature rise ($T_s - T_2$) but is within the stated accuracy of 1 percent of T_2 . The present work contains many parameters and plots not found in reference 9; on the other hand, reference 9 presents equilibrium composition of the normal shock gas, which is not given herein.

The present work provides tabulated hypersonic-flow properties, including electron concentration, in terms of velocity and altitude for the aforementioned characteristic regions about a body in flight in the earth's atmosphere over a large range of flight conditions shown in the following figure.



The range of flight velocities is such as to encompass those beginning where flow tabulations for $\gamma = 1.40$, such as those of reference 10, cease to be applicable (that is, about 3,500 feet per second) up to values corresponding to reentry from planetary missions. This range is obtained by using thermodynamic input data (ref. 4) over the temperature range of 800°K through $14,000^\circ\text{K}$. The range of flight altitudes selected is such as to include that region of the earth's atmosphere wherein it is believed that significant aerodynamic forces or thermal influences of the atmosphere, with respect to the design requirements of the mission, will be experienced by a body in flight. In view of the nature of the atmospheric property variations (ref. 11), twelve altitudes ranging from 36,000 to 323,000 feet are used.

SYMBOLS

- a velocity of sound, ft/sec
- \bar{c}_e mean thermal electron velocity, cm/sec

D	dissociation energy per mole
f	signal frequency, per sec
f_p	plasma frequency, $8,970\sqrt{N_e}$, sec^{-1} (critical frequency)
g	acceleration due to gravity
H	enthalpy per mole
h	enthalpy per unit mass, $\frac{H}{m}$
J	parameter defined in equation (12)
$K()$	ratio of the real-gas to the ideal-gas value of the bracketed parameter for the given M_1
m	molecular weight per mole
M	Mach number, $\frac{u}{a}$
n_0	Lochschmidt's number
N	specie particle concentration, per cm^3
p	pressure
Q	effective cross-section for momentum exchange with electron, cm^2
Q_c	coulomb (ion) cross-section for momentum exchange with electron, cm^2
\bar{Q}_n	average effective neutral cross section for momentum exchange with electron, cm^2
R	gas constant per mole (universal)
s	entropy per unit mass, $\frac{S}{m}$
S	entropy per mole
S^0	entropy at standard pressure per mole
T	temperature, $^{\circ}\text{K}$ or $^{\circ}\text{R}$
u	fluid velocity, ft/sec
V	volume per mole

x	specie mole fraction, $\sum_1 x_i = 1.0$
Z	compressibility factor, $\frac{m_0}{m}$
α	mole fraction of oxygen photodissociated
γ	specific heat ratio
$\gamma_{T,p}$	parameter defined in equation (12)
γ^*	isentropic exponent (eq. (7))
ρ	mass density, $\frac{m}{V}$
σ	electrical conductivity, sec^{-1} (esu) or mho/cm
ν	electron collision frequency
ω	angular signal frequency, $2\pi f$, radians/sec
ω_p	angular plasma frequency, $2\pi f_p$, radians/sec

Subscripts:

0	standard conditions ($p = 1$ atmosphere, $T = \text{ice point}$)
1	ambient conditions
2	behind normal shock
a	dissociated atoms
dc	direct current ($\omega = 0$)
e	electron
i	species in mixture
OA	oxygen in standard air
s	stagnation behind shock
t	total
w	wake, equilibrium inviscid flow
fw	frozen wake, inviscid flow

METHOD OF COMPUTATION

Normal Shock

The computation of the normal-shock flow properties follows that of reference 6 in which the conservation equations for mass, momentum, and energy are used:

$$\rho_1 u_1 = \rho_2 u_2 \quad (1)$$

$$p_1 + \rho_1 u_1^2 = p_2 + \rho_2 u_2^2 \quad (2)$$

$$h_t = h_1 + \frac{u_1^2}{2} = h_2 + \frac{u_2^2}{2} \quad (3)$$

along with the equation of state

$$\frac{p}{\rho} = \frac{ZRT}{m_0} \quad (4)$$

Solution of these equations results in the following relation:

$$\left(\frac{p_2}{p_0} - \frac{p_1}{p_0} \right) \left(\frac{1}{\rho_1/\rho_0} + \frac{1}{\rho_2/\rho_0} \right) = 2 \left(\frac{h_2}{\frac{R}{m_0} T_0} - \frac{h_1}{\frac{R}{m_0} T_0} \right) \quad (5)$$

since $Z_0 = 1.0$.

For given input values of $h_1/\frac{R}{m_0} T_0$, p_1/p_0 , and ρ_1/ρ_0 (corresponding to ambient-air properties at a given altitude), and for a given value of T_2 , equation (5) is iterated until the solutions for $h_2/\frac{R}{m_0} T_0$, ρ_2/ρ_0 , and p_2/p_0 are consistent also with the thermodynamic air properties at this temperature. The ambient-air properties as a function of altitude are taken from reference 11 and are listed in table I. The thermodynamic properties for high-temperature air are taken from reference 4, and interpolation of these tables to satisfy equation (5) is accomplished by linear interpolation of the logarithms of ρ_2/ρ_0 , p_2/p_0 , and $h_2/\frac{R}{m_0} T_0$ at a given temperature.

The flight velocity u_1 is then found by substitution into equations (1) and (2) or (3) the total enthalpy $h_t/\frac{R}{m_0} T_0$ from equation (3), and the flight Mach number M_1 is found by using the values for a_1 listed in table I and taken from reference 11. The velocity u_2 is not tabulated but is readily found from equation (1). The compressibility factor Z_2 and the entropy $s_2/\frac{R}{m_0}$ are found by interpolation of the air tables (ref. 4). The ratios of real-gas to ideal-gas parameters $K(\)$ are found by using ideal-gas values from reference 10 for the same value of flight Mach number M_1 .

The velocity of sound behind the normal shock a_2 is found from interpolation of values for a_2 listed in reference 5 as a function of temperature and density. The computation of velocity of sound in reference 5 is made by using the following relations:

$$a^2 = \gamma^* \frac{P}{\rho} = \gamma^* \frac{R}{m_0} TZ \quad (6)$$

$$\gamma^* = \left(\frac{\partial \log p}{\partial \log \rho} \right)_s \quad (7)$$

The isentropic exponent γ^* is found in reference 5 by use of a spline fit method for obtaining slopes (eq. (7)) from the tabulated thermodynamic data. The basic data used were those of reference 4. It is to be particularly noted that the exponent γ^* is not to be confused with the ratio of specific heats γ . These parameters become identical only for the case of a nonreacting gas, such as air below temperatures of about 1,800° K. This exponent γ^* is also different from the "effective" specific-heat ratio for shock density ratio found in references 7 and 12. The isentropic exponent for air may also be found from a plot in reference 13. This parameter was taken from interpolation of the data of reference 5.

The electron concentration $N_{e,2}$ is computed from the following relation:

$$N_{e,2} = x_{e,2} n_0 \frac{P_2/P_0}{T_2/T_0} = x_{e,2} n_0 Z_2 \frac{\rho_2}{\rho_0} \quad (8)$$

where $x_{e,2}$ is the electron mole fraction and is taken from plots of x_e as a function of ρ/ρ_0 and T . These x_e data were taken from reference 3 for the temperature range 3,000° K to 10,000° K, since the more accepted value for NO ionization energy is used in reference 3. For temperatures below 3,000° K, the

data of reference 14 were used, and for temperatures above 10,000° K, cross plots of the data of references 1 and 3 were used. It should be noted that T_0 and ρ_0 in reference 3 are slightly different from those used herein.

Stagnation Point

The stagnation-point pressure was computed on the basis of an incompressible total pressure for the normal-shock flow:

$$\frac{p_s}{p_2} = \frac{p_2 + \frac{1}{2} \rho_2 u_2^2}{p_2} \quad (9a)$$

and with a further approximation for $p_1 \ll p_2$:

$$\frac{p_s}{p_2} \approx \frac{\frac{\rho_2}{\rho_1} - \frac{1}{2}}{\frac{\rho_2}{\rho_1} - 1} \quad (9b)$$

Equation (9a) can be expressed in terms of the flight parameters and shock-density ratio in the relation

$$\frac{p_s}{p_1} = 1 + \gamma_1 M_1^2 \left(1 - \frac{1}{2} \frac{\rho_1}{\rho_2} \right) \quad (10)$$

These relations were obtained by using also equations (1), (2), (4), and (6). Although equations (9) and (10) are not precisely correct for this compression process, they are numerically convenient, and the results are at least as accurate as can be obtained by reading a Mollier air chart using $h_t/\frac{R}{m_0} T_0$ and $s_2/\frac{R}{m_0}$, the correct method, and more accurate than can be obtained in the case of Newtonian impact pressure from equation (2).

The stagnation-point temperature is again computed from an approximate relation which is numerically convenient and superior to chart reading. This relation

$$\frac{T_s}{T_2} \approx 1 + \frac{J}{2 \left(\frac{\rho_2}{\rho_1} - 1 \right)} \quad (11)$$

is obtained by using equation (9b) and assuming that the relation

$$J = \frac{\gamma_{T,p} - 1}{\gamma_{T,p}} = \left(\frac{\partial \log_e T}{\partial \log_e p} \right)_s \quad (12)$$

is the constant exponent for the compression from normal shock to stagnation in the following isentropic process:

$$\left. \begin{aligned} T &\propto p^J \\ \frac{\Delta p}{p} &\ll 1.0 \\ \frac{\Delta T}{T} &\ll 1.0 \end{aligned} \right\} \quad (13)$$

The parameters $\gamma_{T,p}$ and J are tabulated in reference 15 for argon-free air and $\gamma_{T,p}$ is plotted herein for illustration.

It should be noted that equation (11) is obtained by using an effective constant value of local specific heat for the process J^{-1} . In reference 7 the computation was made on the assumption that the effective value of specific heat for the process was the nondimensional enthalpy (that is, H/RT). However, this assumption leads to errors in some cases of over 50 percent in the temperature change ($T_s - T_2$) for the process, since if only the local specific heat is constant, $\frac{dH}{dT} \neq \frac{H}{T}$ for the case of real air.

Equilibrium Wake

Tabulations are included also for conditions in the far wake of a body for the case of the normal-shock streamline isentropically expanded to ambient pressure, in thermochemical equilibrium and without viscosity. Values of the density ρ_w and temperature T_w were found by plotting the thermodynamic air data of reference 4 in the form p/p_0 as a function of $s/\frac{R}{m_0}$ and reading ρ_w/ρ_0 and T_w at values of the ambient pressure p_1/p_0 and the normal-shock entropy $s_2/\frac{R}{m_0}$, which is the entropy appropriate to this expansion. The values of $x_{e,w}$ for the wake were found from the plots of x_e as a function of ρ/ρ_0 , by reading $x_{e,w}$ at values of ρ_w/ρ_0 and T_w (the wake conditions). Values of $N_{e,w}$ were computed from equation (8) rewritten in terms of the wake parameters $x_{e,w}$, p_1/p_0 , and T_w/T_0 .

Frozen Wake

Computation of an inviscid frozen-wake temperature $T_{f,w}$ and electron concentration $N_{e,f,w}$ was obtained by the following approximate method: The gas composition was assumed to be frozen at the normal-shock equilibrium value and

was then expanded isentropically from normal-shock pressure p_2/p_0 to the far-wake ambient pressure p_1/p_0 by using an effective specific heat for the non-reacting gas mixture (which is, of course, far from an equilibrium composition in the wake) in which the internal energies of the species are assumed to be in equilibrium with the temperature.

The effective specific heat for the process was taken as an average between the initial (shock) and iterated final (wake) values, these temperature-dependent values being computed without regard to reaction energies (since they do not take part in the process) but with the internal energies assumed in equilibrium (coupled) with the translational temperature. The electron concentration $N_{e, fw}$ was then found from equation (8), by use of the wake temperature T_{fw} , pressure p_1/p_0 , and the normal-shock electron mole fraction $x_{e, 2}$, since the composition was frozen at this value.

RESULTS

The computations were carried out according to the methods previously presented for a range of altitudes from 35,900 to 322,900 geopotential feet. Twelve altitudes were selected and include the six altitudes at the boundaries of the three isothermal layers of the earth's homosphere. The ambient properties as a function of altitude were taken from reference 11, except for enthalpy and entropy which were taken from reference 16 for pressure altitudes up to 294,800 feet, and for enthalpy, entropy, and sound velocity at 322,900 feet which were computed by the methods given in the appendix. These ambient properties are listed in table I and are plotted in figures 1 to 4. Figure 5 is presented to show the comparison of ambient properties from reference 11 (1959 ARDC model atmosphere) with the previous model atmosphere (ref. 17), and with a proposed revision to the model. (See table II and refs. 18 and 19.) A list of constants for use with the tables is given in table III.

The results of the hypersonic-flow-property computations are given in table IV, where the parameters at each selected altitude are tabulated at 33 temperatures for the range from 800° K to 14,000° K. Table IV lists 33 parameters including those for normal-shock, stagnation point, and wake conditions for equilibrium and frozen inviscid flow. The parameters tabulated include, in addition to the thermal properties and sound and flow velocities, the electron concentrations for equilibrium and frozen flows. These latter parameters are useful in plasma computations such as those used for the radio-transmission problem. Some of the more widely used thermodynamic parameters from table IV are plotted in figures 6 to 15 as a function of both velocity and altitude. The electron concentration for the three regions tabulated is plotted in figure 16 as a function of velocity and altitude, with values of plasma frequency f_p also shown. For convenience in rapidly estimating the plasma frequencies encountered during various reentry trajectories, the data from figure 16 are cross-plotted in figure 17 on a velocity-altitude plot showing lines of constant plasma frequency. The parameter $\gamma_{T, p}$ taken from reference 15 is plotted in figure 18 as a function

of T and $s/\frac{R}{m_0}$ for use in estimating isentropic flow changes in the real-gas equilibrium shock-heated flow regions. The thermodynamic air data used for these computations included data from reference 16 for the temperature range 800°K through $1,200^\circ\text{K}$ and from references 1, 3, 4, 5, 14, and 15, for the higher temperatures, as discussed previously.

Reliability of Results

Computational accuracy.- For a given set of input values, the accuracy of the parameters computed and tabulated in table IV will be in the range of 0.1 to 0.2 percent, generally. The iteration of equation (5) was not carried further than this accuracy, since the uncertainty in the ambient-air-property input data does not warrant additional precision.

Applicability of results.- All the input data used in the computations, for both the ambient air and the high-temperature air, is with argon included and is therefore consistent and comparable with the data in the general literature for air. The change in the value of the parameters tabulated herein for air from the values in reference 6 on the basis of argon-free air is approximately 0.2 to 0.4 percent for the same model atmosphere.

It can be seen in figures 6(a) and 7(a) that for temperatures of $1,600^\circ\text{K}$ and below (velocities of about 6,000 ft/sec and below) the air composition does not change in the shock-compression process. Consequently, ideal-gas relations (that is, relations for a thermally perfect but calorically imperfect gas) can be used in this range. (See ref. 10.) For temperatures above this range, the so-called real-gas effects become significant, and change of air composition must be taken into account. For temperatures below 800°K (velocities below about 3,500 ft/sec) it can be seen from table IV or from figures 8(a) and 10(a), and also from figure 4 of reference 13 (γ^* as a function of $h/\frac{R}{m_0} T_0$) that ideal-gas relations with constant specific-heat ratio of 1.40 may be used (ref. 10) with only a few percent (<3 percent) error in the results.

The results in table IV are presented in terms of the normal-shock properties; however, the results may be applied also to oblique-shock conditions if the shock angle or the normal component of the flow is specified. (See ref. 6 for procedure; also see refs. 7, 8, 12, and 20.)

Since the computations have been made for only the limiting nonequilibrium conditions - that is, infinite reaction rates (equilibrium) or zero recombination rates (frozen) - the parameters will not be applicable to finite-rate nonequilibrium problems. In many cases, however, these limiting-rate parameters serve to bracket the actual finite-rate problem and thereby provide a means for rapid estimation of the magnitude of the effects of nonequilibrium. At flight altitudes below about 100,000 feet (depending also on body scale) the flow will generally be close to thermochemical equilibrium around typical bodies, and therefore the tabulated data should generally apply for these altitudes. For flight at higher altitudes (up to, say, 200,000 feet) the characteristic reaction

lengths for the stagnation streamline of blunt bodies are about equal to the shock standoff distance, so that for this streamline the equilibrium computations should apply near the stagnation point. For other streamlines (oblique shock streamlines), however, neither equilibrium nor frozen-flow computations apply, and thus finite-rate nonequilibrium computations are needed in this altitude range. It is also a good approximation, in the case of the stagnation streamline, to assume a frozen-flow composition (no recombination) in the expansion of this flow about the body and into the wake for these altitudes; and thus the frozen-wake computations should have at least qualitative application in this range. For still higher altitudes, nonequilibrium reactions may extend throughout the flow field, including the stagnation point, and require employment of finite-rate chemical kinetics.

For the altitude range encompassed by the present tabulations, the shock-layer flow around typical bodies is considered to be in the continuum flow regime of fluid mechanics (to a lesser extent dependent on the velocity range) so that the computations of the tabulated parameters are valid in this regard. It must be remembered, however, that for altitudes of the order of 250,000 feet and higher (depending also on scale) the viscous effects in the shock layer become very large - that is, boundary-layer thickness is of the same order as the shock-layer thickness. For this reason, as well as because of the nonequilibrium aspect of the flow, tabulations of inviscid flow properties are not applicable in this range other than to serve as guidelines to more comprehensive computations.

Effects of Ambient-Air-Property Uncertainties

Knowledge of the ambient properties of the earth's atmosphere is being constantly revised, supplemented, and extended as a result of improved measurement techniques and conceptual changes. While these revisions are of a greater magnitude in that part of the atmosphere above the homosphere (above 295,000 feet), the changes have been significant at altitudes even as low as the troposphere (65,000 feet). The ambient-air properties used in the present work were taken from reference 11 (1959 model), which had replaced reference 17 (1956 model) as a model atmosphere, and these properties have already been superseded to a certain extent. (See refs. 18 and 19, table II, and fig. 5 for latest revision.) There have been many other proposed atmospheric models. It is well, then, to consider the magnitude of these changes, the effects of such changes on the hypersonic flow parameters presented, and the other uncertainties involved in application of the results to a particular situation.

Ambient temperature.- The maximum change in ambient temperature in the homosphere from the 1956 to the 1959 model atmosphere is in the mesopause and is about 30° K. (See fig. 5.) The revision is within 15° K of the 1959 model. The latter figure amounts to a change in the ambient enthalpy of about $0.2 \frac{R}{m_0} T_0$, which in comparison with the kinetic energy term in equation (3) for typical velocities is generally only a small fraction of a percent. This small change indicates that for a given flight velocity, the error in normal-shock temperature will be very small due to this ambient temperature change. The error is

also small for most of the other parameters including the $K()$ parameters, with the exception of those involving ratios of temperatures or those directly dependent upon T_1 , for example, T_2/T_1 and M_1 . In these parameters

the errors could be much higher, that is, as much as 9 percent for the $15^\circ K$ case, so that correction to these parameters would be necessary, but can be generally avoided by employment of the parameters of lesser dependency. For example, the pressure ratio p_2/p_1 at a given flight velocity is also strongly dependent on an ambient temperature change; however, at a given flight Mach number there is little or no dependency. In order to account for the change in p_2/p_1 due to a change in T_1 , therefore, the value of M_1 is correspondingly changed ($a_1 \propto T_1^{1/2}$) and the new p_2/p_1 found from the tables as based on the corrected M_1 (or a plot of M_1 as a function of p_2/p_1).

Ambient pressure.- Changes in ambient pressure from the 1956 (ref. 17) to the 1959 (ref. 11) model are found at altitudes above 200,000 feet and at the highest altitudes tabulated herein are of the order of 50 percent of the 1956 values. (The revision lies much closer to the 1959 model.) The physical result of the lower ambient pressure on the shock-heated flow properties is that additional dissociation occurs at the lower pressure level and this results in lower temperatures for a given flight velocity. The effect of this change is not significant below flight velocities of about 30,000 feet per second, but will result in temperatures that are as much as two percent lower for higher flight velocities at the high altitudes where the pressure changes are large. This can be seen from equation (3) along with the high-temperature air properties tables (ref. 4) where the total enthalpy at constant u_1 is unchanged due to p_1 changes but the lower pressure levels result in larger Z 's and lower T 's in the high-temperature regions. Most of the other parameters are influenced to a somewhat lesser degree by the change, although ρ_2/ρ_1 will be changed by about the same amount. Note, however, that the pressure changes from the 1959 model (ref. 11) to the latest revision (ref. 18) are much smaller than those discussed here, so that the parameters as tabulated herein will be within 1 percent in all cases, and generally better than this.

Ambient composition.- While the composition of the homosphere is constant, the variation of composition above this point (295,000 feet) does not seem to be firmly established. Photodissociation of the ambient O_2 due to U.V. absorption occurs in the thermosphere, and while the ratio of O/N atoms (that is, conservation of total atoms in a reaction process) is believed to remain about constant in the region between 290,000 and 400,000 feet due to diffusion and mixing, the molecular weight is different from standard air and varies with the amount photodissociated. Figure 5 shows that a large change of m_1 occurred from the 1956 to the 1959 model. The later revision (ref. 19) lies somewhere in between these models in this region. Computation of the effects of composition on ambient enthalpy, entropy, and sound velocity is discussed in the appendix.

At the highest altitude tabulated herein (323,000 feet) a little over 1 percent of the ambient oxygen is photodissociated according to the 1959 model atmosphere (see appendix). This produces an increase in the ambient enthalpy of about

$0.5 \frac{R}{m_0} T_0$ over that for a case of no photodissociation. This chemical energy which is stored in the atmosphere results in increased stagnation enthalpy for a given flight velocity and thus increases the temperatures in the shock-heated gas. For the case of 1-percent photodissociated ambient oxygen, the increase is only about 0.1 percent of typical stagnation enthalpies, but could be much higher if compositions are found to be more greatly photodissociated.

It should be pointed out that since the O/N atom ratio is assumed the same as normal air in this altitude region, one can continue to use the tabulated high-temperature air properties, such as reference 4, since these are based on this same ratio. It is necessary to revise only the ambient-air properties of enthalpy, entropy, et cetera (as a result of this photodissociation), which are inputs to the flow computations. (See table I.)

Other factors.- A number of other factors which may affect the reliability of the tabulated parameters as a result of uncertainties in the ambient-air input properties should be considered. For example, high-altitude winds are known to exist in the atmosphere and are not specifiable for a particular time or location. Reported wind velocities do not indicate, however, that significant effects on the tabulated flow parameters are to be expected. Other uncertainties that exist in the ambient-air properties are attributable to seasonal, geographical, temporal, and diurnal variations from the effective average values used in the standard. These factors can in many cases introduce deviations from the standard which are larger than the differences between atmospheric models.

Omission of Collision Frequency and Conductivity From the Tables

In addition to the electron concentration, the electron collision frequency and the electrical conductivity of a plasma - or in the case of reentry flow fields, of a lossy dielectric medium - are of interest in the radio communications problem and to magnetoplasma dynamics work. These parameters were not included in the computations of the tables because of the large uncertainty in the collision cross section for momentum transfer in electron-atom encounters in air species. There is a resulting uncertainty by a factor of roughly 3 in these parameters in the temperature range where the atom fraction is appreciable and the ion fraction not yet significant. There is, in fact, an uncertainty in the electron-molecule interaction data for air in the lower temperature range. For general utility, however, plots of collision frequency and electrical conductivity are presented. These values are based on a simplified plasma model which yields results within a factor of 2 of those using more refined methods, but use of this model is justifiable in view of the uncertainty (of the same magnitude) in the interaction data.

By use of the general relation for collision frequency

$$\nu = \bar{c}_e \sum_i N_i Q_i \quad (14)$$

the following approximations are made. The collision cross sections for electron encounters with all the neutral species are lumped into one effective average value \bar{Q}_n . The ions in the mixture are assumed to be singly ionized only (considered applicable up to $T \approx 15,000^\circ$ K), and electron-electron encounters are neglected. The electrons are assumed to have a Maxwellian velocity distribution at the gas temperature. Equation (14) is then written in terms of mole fraction and by substitution for \bar{c}_e and the various physical constants yields

$$\nu = 4.56 \times 10^{27} \frac{p/p_0}{T^{1/2}} \left[x_e Q_c + (1 - 2x_e) \bar{Q}_n \right] \quad (15)$$

which is herein evaluated by using \bar{Q}_n as a constant having a value 7×10^{-16} square centimeters, and computing Q_c (the coulomb, or ion, cross section) from the impact parameter and the Debye shielding distance in a manner to account also for close encounters similar to that used in reference 21. The results are plotted in figure 19 for the three flow regimes; and in figure 17 lines of constant $\frac{\nu}{\omega_p} = \frac{\nu}{2\pi f_p}$ are plotted by using these results. It is seen

from equation (15) that for very small values of x_e ($x_e \ll \frac{\bar{Q}_n}{Q_c} \approx 10^{-2}$), equation (15) reduces to

$$\nu = 3.2 \times 10^{12} \frac{p/p_0}{T^{1/2}} \quad (16)$$

when \bar{Q}_n is equal to 7×10^{-16} square centimeters. This relation is useful in the lower temperature range (or in the low x_e -range) where the long-range (coulomb) forces are insignificant.

Based on these collision frequency values, the electrical conductivity has been computed and is plotted in figure 20 for expediency in plasma work. This computation is made from the low-frequency conductivity relation,

$$\sigma = \frac{\omega_p^2 \nu}{4\pi(\omega^2 + \nu^2)} \quad (17)$$

which is then qualified for the case of $\omega = 0 = 2\pi f$ (d-c) for convenience in plotting. If the conversion constant from sec^{-1} (esu) to mho/cm is used, equation (17) then becomes, for the direct-current case plotted:

$$\sigma_{dc} = 2.81 \times 10^{-4} \frac{N_e}{\nu}, \text{ mho/cm} \quad (18)$$

The alternating-current conductivity is then readily obtained by using the σ_{dc} values from the plots and applying the following relation derived from equation (17):

$$\sigma = \sigma_{dc} \left[\frac{1}{1 + \left(\frac{\omega}{\nu}\right)^2} \right] \quad (19)$$

CONCLUDING REMARKS

Real-air hypersonic-flow parameters are presented in tabular and graphical form for flight in the earth's atmosphere as a function of flight velocity and flight altitude. Thermochemical equilibrium flow properties are given for the inviscid normal shock and stagnation point, and both equilibrium and frozen-flow parameters, including electron concentration, are listed for the far wake of the inviscid stagnation streamline. The tabulations are made for twelve flight altitudes ranging from 35,900 feet to 322,900 feet and for flight velocities and shock-heated gas temperatures encompassing those encountered in return from planetary missions. Included are discussions of the applicability of the computed parameters to a given problem, and effects due to the uncertainties in the input data for ambient air.

Langley Research Center,
National Aeronautics and Space Administration,
Langley Station, Hampton, Va., November 9, 1962.

APPENDIX

AMBIENT PROPERTIES IN LOWER THERMOSPHERE

Enthalpy

For the case where normal air has been photodissociated (as in the lower thermosphere, ref. 22) the relation

$$Z_1 = \frac{m_0}{m_1} = 1 + \alpha x_{OA} \quad (A1)$$

represents the molecular weight ratio (compressibility factor) in terms of the fraction of oxygen dissociated α . The term αx_{OA} is the fraction of the air molecules dissociated where $x_{OA} = 0.20946$ from table III. It is immediately shown from equation (A1) and table I that at 322,900 feet altitude, α is 0.0115 for $Z_1 = 1.0024$. The mole fraction of dissociated atoms in the mixture (for this case, oxygen atoms only) is given by

$$x_a = \frac{2(Z - 1)}{Z} \quad (A2)$$

and the balance of the species in the mixture ($1 - x_a$) consists mainly of O_2 and N_2 molecules. The enthalpy of an ideal dissociated gas mixture may be written

$$\frac{h}{\frac{R}{m_0} T_0} = Z \sum_i x_i \left(\frac{H}{RT_0} \right)_i \quad (A3)$$

and that part of the term $\left(\frac{H}{RT_0} \right)_i$ due to the dissociated atoms in the mixture is

$$\left(\frac{H}{RT_0} \right)_a = \left(\frac{H}{RT_0} \right)_{\text{thermal}} + \frac{1}{2} \frac{D_0}{RT_0} \quad (A4)$$

where the last term in equation (A4) is the chemical part of the enthalpy. The contribution in equation (A3) due to the chemical term (O atoms only in this case) is, then

$$\frac{1}{2} \frac{D_0}{RT_0} Z x_a = \frac{\alpha x_{OA} D_0}{RT_0} = 45.5\alpha \quad (A5)$$

where $\frac{D_0}{RT_0} = 217$ (5.11 ev) for the oxygen dissociation energy. (See ref. 22.)

It is seen from equation (A5) that for $\alpha = 0.0115$ the chemical energy stored in

the atmosphere due to photodissociation at 322,900 feet is about $0.52 \frac{R}{m_0} T_0$, based on the 1959 model atmosphere. The enthalpy of the ambient dissociated air was determined and tabulated in table I, by using equation (A3), and the ideal gas species data from reference 16.

Entropy

The entropy for an ideal dissociated gas mixture may be expressed as

$$\frac{s}{R/m_0} = Z \sum_i x_i \left(\frac{S}{R} \right)_i = Z \sum_i x_i \left[\left(\frac{S^0}{R} \right)_i - \log_e \left(\frac{p}{p_0} \right)_i \right] \quad (A6)$$

where

$$\left(\frac{p}{p_0} \right)_i = x_i \frac{p}{p_0} \quad (A7)$$

and S^0/R is the species entropy at standard pressure. Combining and expanding the above relations and noting that $\sum_i x_i = 1.0$ yields:

$$\frac{s}{R/m_0} = Z \left[\sum_i x_i \left(\frac{S^0}{R} \right)_i - \sum_i x_i \log_e x_i - \log_e \frac{p}{p_0} \right] \quad (A8)$$

Using this relation and the ideal gas species properties from reference 16, the entropy for ambient dissociated air at 322,900 feet altitude was computed and tabulated in table I. It should be mentioned that for this case of $\alpha = 0.0115$, the entropy is almost identically the same as undissociated air at this pressure and temperature.

Velocity of Sound

The velocity of sound above the homosphere is not tabulated in reference 11 but may be found from the scale height, which is tabulated therein, if the isentropic exponent γ^* is known. The scale height is expressible as (see ref. 11)

$$\text{Scale height} = \frac{R}{m_0} \frac{TZ}{g} \quad (A9)$$

where the product TZ is the molecular scale temperature. Combining equation (A9) with equation (6) results in the relation

$$a^2 = \gamma^* g \times \text{Scale height} \quad (A10)$$

where g is the acceleration due to gravity at the specified altitude. The value of γ^* for a dissociated mixture is found from equation (7), but for this case of photodissociated ambient air no computations or tabulations are found in the literature. However, an exponent may be assumed on the basis that the small pressure perturbation process for this gas would behave thermally as in a non-reacting gas mixture of this ambient composition (that is, photodissociation considered nonthermal). In effect this is an assumption of frozen-flow composition, and a value of specific-heat ratio γ is computed as for an ideal nonreacting gas mixture.

For the case of $\alpha = 0.0115$ at an altitude of 322,900 feet the value for γ^* is very close to that of normal air, being computed to be 1.404. By use of this value, a_1 is computed from equation (A10) and listed in table I.

REFERENCES

1. Gilmore, F. R.: Equilibrium Composition and Thermodynamic Properties of Air to 24,000° K. U.S. Air Force Project RAND Res. Memo. RM-1543, The RAND Corp., Aug. 24, 1955. (Also available from ASTIA as AD 84052.)
2. Hilsenrath, Joseph, and Beckett, Charles W.: Tables of Thermodynamic Properties of Argon-Free Air to 15,000° K. AEDC-TN-56-12, Arnold Eng. Dev. Center, Sept. 1956. (Also available from ASTIA as Doc. No. AD-98974.)
3. Logan, J. G., Jr., and Treanor, C. E.: Tables of Thermodynamic Properties of Air From 3,000° K to 10,000° K at Intervals of 100° K. Rep. No. BE-1007-A-3. Cornell Aero. Lab., Inc., Jan. 1957.
4. Hilsenrath, Joseph, Klein, Max, and Woolley, Harold W.: Tables of Thermodynamic Properties of Air Including Dissociation and Ionization From 1,500° K to 15,000° K. AEDC-TR-59-20, Arnold Eng. Dev. Center, Dec. 1959.
5. Landis, F., and Nilson, E. N.: Thermodynamic Properties of Ionized and Dissociated Air From 1,500° K to 15,000° K. P & WA Rep. No. 1921, Pratt and Whitney Aircraft, Jan. 1961.
6. Huber, Paul W.: Tables and Graphs of Normal-Shock Parameters at Hypersonic Mach Numbers and Selected Altitudes. NACA TN 4352, 1958.
7. Wittliff, Charles E., and Curtis, James T.: Normal Shock Wave Parameters in Equilibrium Air. Rep. No. CAL-111, Cornell Aero. Lab., Inc., Nov. 1961.
8. Batchelder, R. A.: Normal and Oblique Shock Characteristics at Hypersonic Speeds. Eng. Rep. No. LB-25599, Supp. I, Douglas Aircraft Co., Inc., Feb. 16, 1959.
9. Marrone, Paul V.: Normal Shock Waves in Air: Equilibrium Composition and Flow Parameters for Velocities From 26,000 to 50,000 Ft/Sec. CAL Rep. No. AG-1729-A-2 (Contract NASr-119), Cornell Aero. Lab., Inc., Aug. 1962.
10. Ames Research Staff: Equations, Tables, and Charts for Compressible Flow. NACA Rep. 1135, 1953. (Supersedes NACA TN 1428.)
11. Minzner, R. A., Champion, K. S. W., and Pond, H. L.: The ARDC Model Atmosphere, 1959. Air Force Surveys in Geophysics No. 115 (AFCRC TR-59-267), Air Force Cambridge Res. Center, Aug. 1959.
12. Trimpi, Robert L., and Jones, Robert A.: A Method of Solution With Tabulated Results for the Attached Oblique Shock-Wave System for Surfaces at Various Angles of Attack, Sweep, and Dihedral in an Equilibrium Real Gas Including the Atmosphere. NASA TR R-63, 1960.
13. Moeckel, W. E., and Weston, Kenneth C.: Composition and Thermodynamic Properties of Air in Chemical Equilibrium. NACA TN 4265, 1958.

14. Fliskin, J. M., Roberts, C. A., and Sisco, W. B.: Equilibrium Composition of Air Below 3,000 Degrees Kelvin Including Electron Densities. Eng. Rep. No. LB-30078, Douglas Aircraft Co., Inc., Apr. 6, 1959.
15. Hochstim, Adolph R.: Gas Properties Behind Shocks at Hypersonic Velocities. III. Tables of Thermodynamical Properties of Air. ZPh-004, CONVAIR, Aug. 1, 1958 (Revised).
16. Hilsenrath, Joseph, Beckett, Charles W., et al.: Tables of Thermal Properties of Gases. NBS Cir. 564, U.S. Dept. Commerce, 1955.
17. Minzner, R. A., and Ripley, W. S.: The ARDC Model Atmosphere, 1956. Air Force Surveys in Geophysics No. 86 (AFCRC TN-56-204, ASTIA Doc. 110233), Air Force Cambridge Res. Center, Dec. 1956.
18. Anon.: U.S. Standard Atmosphere, 1962. NASA, U.S. Air Force, and U.S. Weather Bureau, Dec. 1962.
19. Champion, Kenneth S. W., and Minzner, Raymond A.: Proposed Revision of U.S. Standard Atmosphere 90 to 700 Km. AFCRL-62-802, Air Force Cambridge Res. Lab., July 1962.
20. Moeckel, Wolfgang E.: Oblique-Shock Relations at Hypersonic Speeds for Air in Chemical Equilibrium. NACA TN 3895, 1957.
21. Lin, Shao-Chi, Resler, E. L., and Kantrowitz, Arthur: Electrical Conductivity of Highly Ionized Argon Produced by Shock Waves. Jour. Appl. Phys., vol. 26, no. 1, Jan. 1955, pp. 95-109.
22. Hord, Richard A.: Properties of the Atmosphere. Reentry Dynamics. Bull. of Virginia Polytechnic Inst., Eng. Exp. Station Ser. No. 150, vol. LV, no. 10, Aug. 1962, pp. 75-92.

TABLE I.- VARIATION OF AMBIENT-AIR PROPERTIES WITH ALTITUDE

Altitude, ft		$T_1,$	$T_1,$	$a_1,$	p_1/p_0	ρ_1/ρ_0	$\frac{h_1}{R T_0}$	$\frac{s_1}{R}$	a_1/a_0	Z_1
Geopotential	Geometric	$^{\circ}K$	$^{\circ}R$	ft/sec			$\frac{m_0}{m_0}$	$\frac{m_0}{m_0}$		
0	0	288	519	1,117	1.000	0.9478	3.68	23.77	1.027	1.000
35,900	36,000	217	390	968	.2250	.2832	2.77	24.28	.891	1.000
59,800	60,000	217	390	968	$.7135 \times 10^{-1}$	$.8995 \times 10^{-1}$	2.77	25.43	.891	1.000
82,200	82,500	217	390	968	$.2438 \times 10^{-1}$	$.3071 \times 10^{-1}$	2.77	26.49	.891	1.000
100,000	100,500	233	420	1,005	$.1067 \times 10^{-1}$	$.1250 \times 10^{-1}$	2.98	27.57	.924	1.000
120,300	121,000	252	453	1,043	$.4462 \times 10^{-2}$	$.4841 \times 10^{-2}$	3.22	28.69	.960	1.000
154,800	156,000	283	509	1,106	$.1161 \times 10^{-2}$	$.1122 \times 10^{-2}$	3.61	30.45	1.017	1.000
173,500	175,000	283	509	1,106	$.5826 \times 10^{-3}$	$.5630 \times 10^{-3}$	3.61	31.17	1.017	1.000
200,100	202,000	247	444	1,034	$.2052 \times 10^{-3}$	$.2271 \times 10^{-3}$	3.15	31.73	.951	1.000
230,400	233,000	205	369	942	$.5042 \times 10^{-4}$	$.6713 \times 10^{-4}$	2.62	32.48	.867	1.000
259,700	263,000	166	298	847	$.9631 \times 10^{-5}$	$.1589 \times 10^{-4}$	2.12	33.40	.779	1.000
294,800	299,000	166	298	847	$.1064 \times 10^{-5}$	$.1755 \times 10^{-5}$	2.12	35.60	.779	1.000
322,900	328,000	199	358	930	$.2119 \times 10^{-6}$	$.2903 \times 10^{-6}$	3.05	37.87	.856	1.0024

TABLE II.- REVISIONS TO STANDARD ATMOSPHERE

ACCORDING TO REFERENCE 18

Geopotential altitude, ft	T ₁ , °K	Change from 1959 model, °K	p ₁ /p ₀	Change from 1959 model, percent	ρ ₁ /ρ ₀	Change from 1959 model, percent
0	288	0	1.000	0	0.948	0
35,900	217	0	.224	-.6	.282	-.6
59,800	217	0	.716 × 10 ⁻¹	.5	.905 × 10 ⁻¹	.5
82,200	222	5	.243 × 10 ⁻¹	-.3	.300 × 10 ⁻¹	-2.3
100,000	227	-6	.107 × 10 ⁻¹	.3	.128 × 10 ⁻¹	2.7
120,300	242	-10	.434 × 10 ⁻²	-2.7	.488 × 10 ⁻²	.7
154,800	271	-12	.107 × 10 ⁻²	-7.5	.108 × 10 ⁻²	-4.5
173,500	269	-14	.518 × 10 ⁻³	-11	.526 × 10 ⁻³	-6.6
200,100	253	6	.180 × 10 ⁻³	-12	.194 × 10 ⁻³	-14
230,400	216	11	.461 × 10 ⁻⁴	-8.5	.582 × 10 ⁻⁴	-13
259,700	181	15	.983 × 10 ⁻⁵	2.1	.148 × 10 ⁻⁴	-6.9
294,800	181	15	.125 × 10 ⁻⁵	18	.189 × 10 ⁻⁵	7.2

TABLE III.- USEFUL CONSTANTS

$$a_0 = 1087.4 \text{ ft/sec, } 331.45 \text{ m/sec}$$

$$g_0 = 32.174 \text{ ft/sec}^2, 980.67 \text{ cm/sec}^2$$

$$m_0 = 28.966 \text{ per mole}$$

$$n_0 = 2.686 \times 10^{19} \text{ per cm}^3 \text{ (Lochs Schmidt's number)}$$

$$p_0 = 2116.2 \text{ lb/ft}^2, 1.0133 \times 10^6 \text{ dynes/cm}^2, 1.0133 \times 10^3 \text{ mb}$$

$$R = 49,722 \text{ ft-lb/slug-mole } ^\circ\text{R, } 1.9873 \text{ cal/mole } ^\circ\text{K}$$

$$\frac{R}{m_0} = 1716.56 \text{ ft-lb/slug } ^\circ\text{R}$$

$$\frac{R}{m_0} T_0 = 844,014 \text{ ft-lb/slug, } 33.86 \text{ Btu/lb}$$

$$T_0 = 491.69 ^\circ\text{R, } 273.16 ^\circ\text{K}$$

$$\rho_0 = 0.002508 \text{ slug/ft}^3, 1.2931 \times 10^{-3} \text{ gm/cm}^3$$

$$1,000 \text{ ft} = 0.3048 \text{ km, } 0.1646 \text{ nautical mile}$$

Normal air composition (mole fraction)

$$\text{N}_2 \quad 0.78084$$

$$\text{O}_2 \quad 0.20946$$

$$\text{Ar} \quad 0.00934$$

$$\text{CO}_2 \quad 0.00033$$

$$\text{Ne} \quad 0.00003$$

TABLE IV.- NORMAL SHOCK PARAMETERS - Concluded

(i) For geopotential altitude of 322,900 ft; $T_1 = 199^\circ \text{K}$; $a_1 = 930 \text{ ft/sec}$; $p = 2.119 \times 10^{-7} \text{ atm}$

T_2 , $^\circ\text{K}$	u_1 , ft/sec	M_1	Z_2	$\frac{P_2}{P_1}$	$K(P_2)$	$\frac{P_2}{P_0}$	$\frac{P_2}{P_1}$	$\frac{P_2}{P_1}$	$K(P_2)$	$\frac{P_2}{P_0}$	$\log \frac{P_2}{P_0}$	$\frac{\rho_2}{\rho_0}$	$\frac{T_2}{T_1}$	$K(T_2)$	$T_{s,}$ $^\circ\text{K}$	$T_{w,}$ $^\circ\text{K}$	$T_{fw,}$ $^\circ\text{K}$
2,000	7.659×10^3	8.223	1.034	84.00	1.067	1.78×10^{-5}	89.80	8.082	1.447	0.2351×10^{-5}	-5.629	10.05	0.7133	2,013	---	663	
2,200	9.295	9.977	1.092	127.2	1.097	2.696	133.8	10.54	1.845	.3066	-5.513	11.06	.5446	2,206	---	619	
3,000	12.41	13.33	1.210	230.1	1.111	4.875	239.8	12.61	2.162	.3670	-5.435	15.08	.4250	3,029	---	647	
3,400	13.10	14.07	1.219	255.6	1.108	5.417	266.7	12.27	2.097	.3571	-5.447	17.09	.4334	3,421	---	711	
4,000	15.83	17.00	1.304	377.5	1.121	8.00	391.3	14.40	2.442	.4190	-5.378	20.10	.3520	4,009	---	685	
4,400	19.61	21.05	1.472	587.5	1.137	1.245×10^{-4}	604.3	18.05	3.042	.5251	-5.280	22.11	.2538	4,407	---	548	
5,000	25.75	27.65	1.827	1,024	1.148	2.170	1,047	22.32	3.744	.6492	-5.188	25.13	.1680	5,008	---	363	
6,000	28.69	30.80	1.993	1,267	1.145	2.685	1,298	21.09	3.533	.6135	-5.212	30.15	.1626	6,033	---	346	
7,000	30.29	32.52	2.044	1,407	1.140	2.981	1,444	19.57	3.277	.5693	-5.245	35.18	.1703	7,022	---	371	
7,500	31.82	34.17	2.110	1,553	1.140	3.290	1,593	19.53	3.268	.5680	-5.246	37.69	.1654	7,517	---	360	
8,000	34.22	36.74	2.227	1,798	1.142	3.810	1,844	20.09	3.360	.5843	-5.233	40.20	.1526	8,015	---	328	
9,000	41.43	44.49	2.659	2,648	1.147	5.610	2,709	22.02	3.679	.6406	-5.193	45.23	.1173	9,014	---	222	
10,000	49.89	53.56	3.267	3,849	1.150	8.156	3,932	23.44	3.914	.6820	-5.166	50.25	$.8993 \times 10^{-1}$	10,024	---	135	
11,000	55.59	59.68	3.725	4,776	1.149	1.012×10^{-3}	4,880	23.20	3.871	.6748	-5.171	55.28	.7971	11,023	---	101	
12,000	58.10	62.38	3.908	5,205	1.147	1.103	5,325	22.09	3.686	.6426	-5.192	60.30	.7961	12,049	---	95	

T_2 , $^\circ\text{K}$	$\frac{a_2}{a_1}$	$K(a_2)$	$\frac{a_2}{a_0}$	M_2	$K(M_2)$	$\frac{h_2}{R/T_0}$	$\frac{h_2}{R/T_0}$	$\frac{s_2}{R/T_0}$	$\frac{s_2 - s_1}{R/T_0}$	$x_{e,2}$	$x_{e,w}$	$N_{e,2}$, per cm^3	$N_{e,w}$, per cm^3	$N_{e,fw}$, per cm^3	γ_2^*
2,000	2.864	0.7630	2.45	0.3552	0.9059	36.52	37.67	43.31	5.44	-----	-----	-----	-----	-----	1.112
2,200	3.075	.6825	2.63	.3079	.7943	52.86	54.02	44.99	7.12	-----	-----	-----	-----	-----	1.103
3,000	4.092	.6870	3.30	.2582	.6734	92.49	93.98	48.72	10.85	8.5×10^{-7}	---	1.0×10^8	---	2.0×10^6	1.294
3,400	4.183	.6662	3.578	.2740	.7157	102.8	104.4	49.47	11.60	5.2×10^{-6}	---	6.1×10^8	---	1.1×10^7	1.180
4,000	4.515	.5975	3.862	.2613	.6854	149.1	151.0	52.35	14.48	3.74×10^{-5}	---	5.5×10^9	---	8.5×10^7	1.094
4,400	5.025	.5384	4.298	.2321	.6106	228.1	230.0	56.85	18.98	8.5×10^{-5}	---	-----	---	2.4×10^8	1.092
5,000	6.019	.4921	5.148	.2059	.5429	391.3	394.5	65.45	27.58	2.65×10^{-4}	---	8.4×10^{10}	---	1.1×10^9	1.110
6,000	7.378	.5418	6.31	.1980	.5223	485.1	488.9	69.85	31.98	3.05×10^{-3}	---	1.0×10^{12}	---	1.4×10^{10}	1.275
7,000	7.693	.5352	6.58	.2160	.5701	540.4	544.6	71.95	34.08	2.50×10^{-2}	---	7.8×10^{12}	---	1.1×10^{11}	1.159
7,500	7.983	.5288	6.828	.2192	.5786	597.0	600.8	73.87	36.00	5.5×10^{-2}	---	-----	---	2.4	1.128
8,000	8.420	.5188	7.202	.2173	.5737	688.8	694.3	76.78	38.91	1.10×10^{-1}	---	3.8×10^{13}	---	5.2	1.116
9,000	9.759	.4969	8.347	.2070	.5470	1,012	1,016	86.16	48.29	2.5	---	1.1×10^{14}	---	1.8×10^{12}	1.115
10,000	11.47	.4851	9.808	.1993	.5267	1,463	1,472	98.06	60.19	3.95	---	2.4	---	4.6	1.129
11,000	13.06	.4959	11.17	.1970	.5209	1,817	1,827	106.6	68.69	4.6	---	3.1	---	7.1	1.166
12,000	14.51	.5271	12.41	.1947	.5147	1,984	1,996	110.2	72.35	4.98	---	3.4	---	8.2	1.258

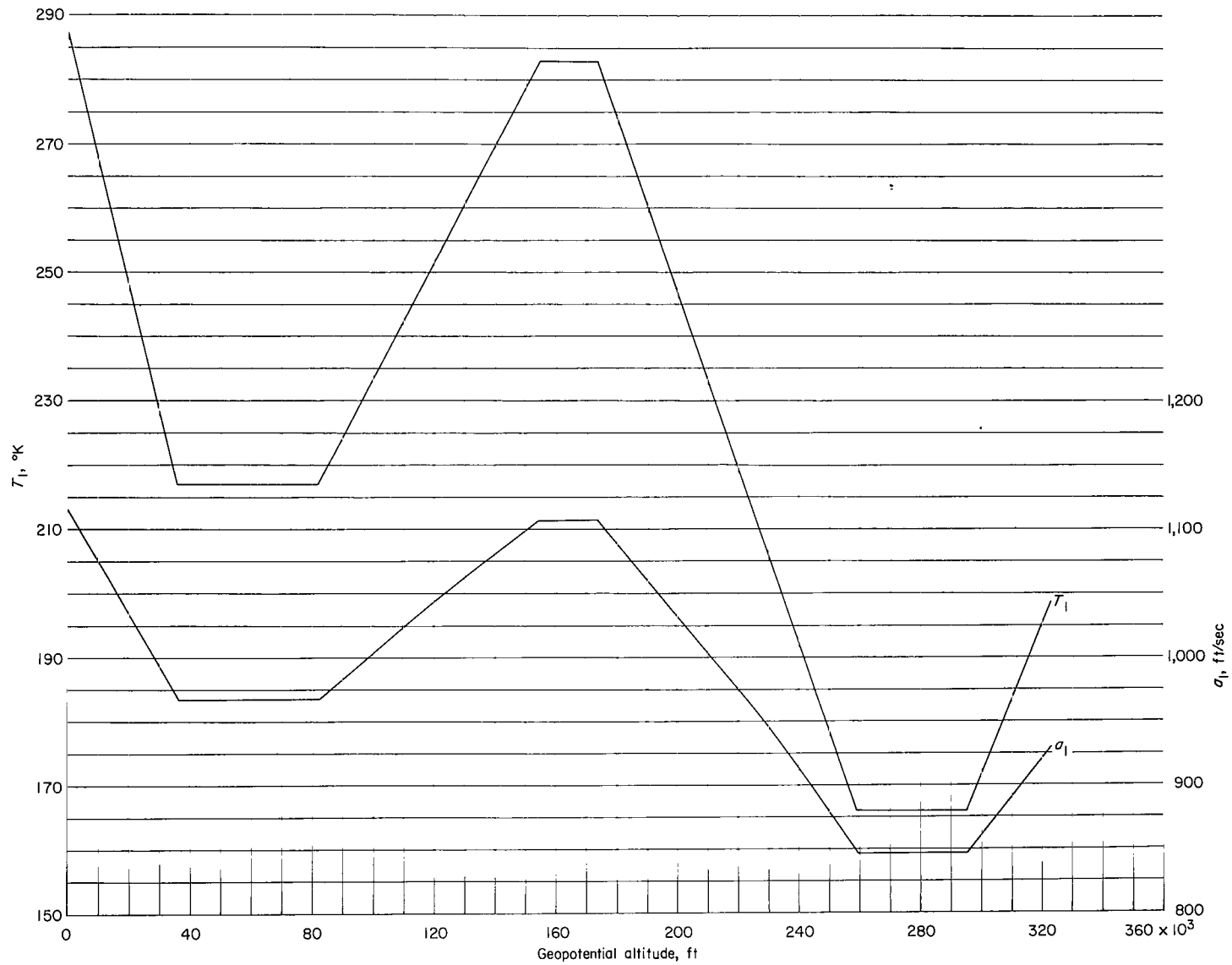


Figure 1.- Variation of ambient temperature and velocity of sound with altitude.

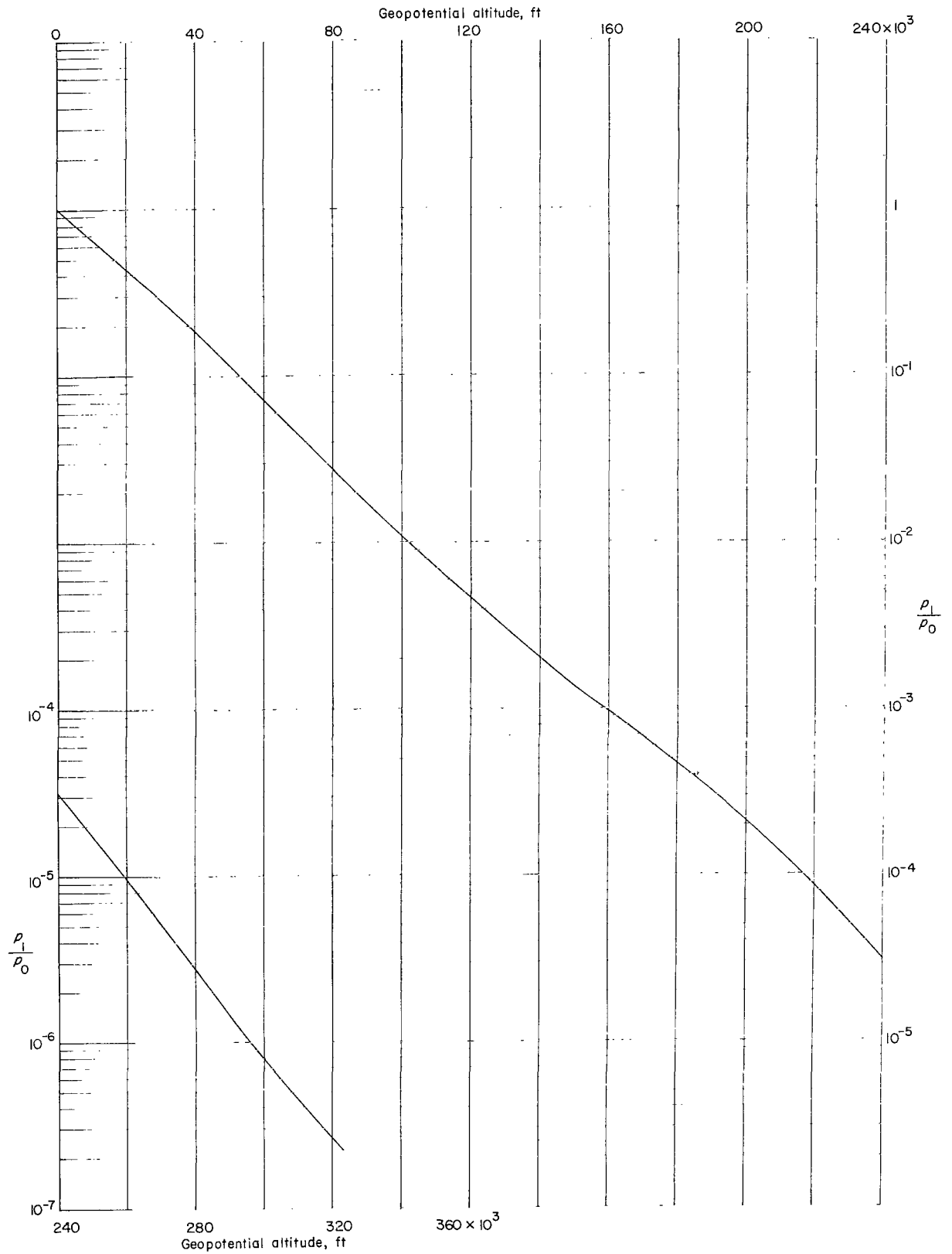


Figure 2.- Variation of ambient pressure with altitude.

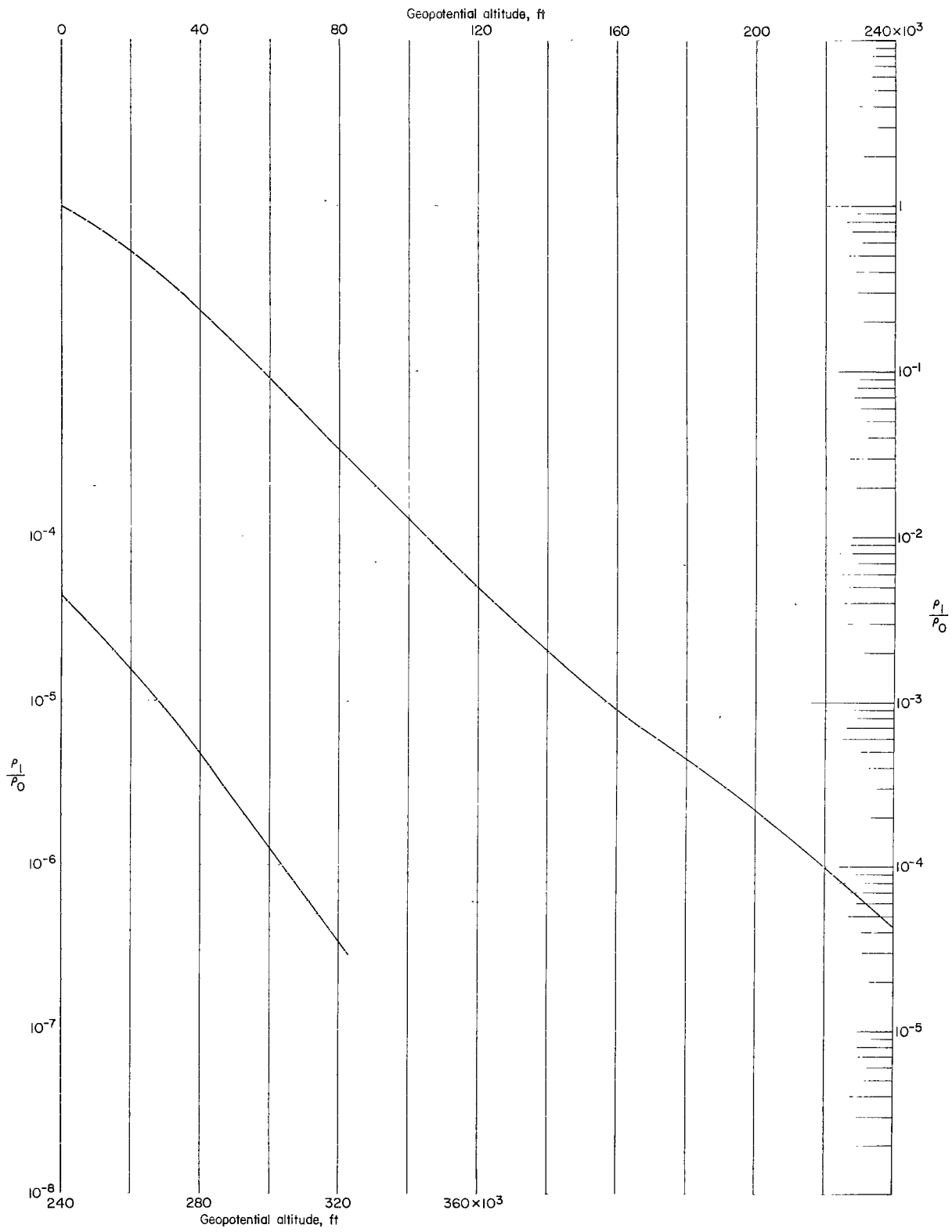


Figure 3.- Variation of ambient density with altitude.

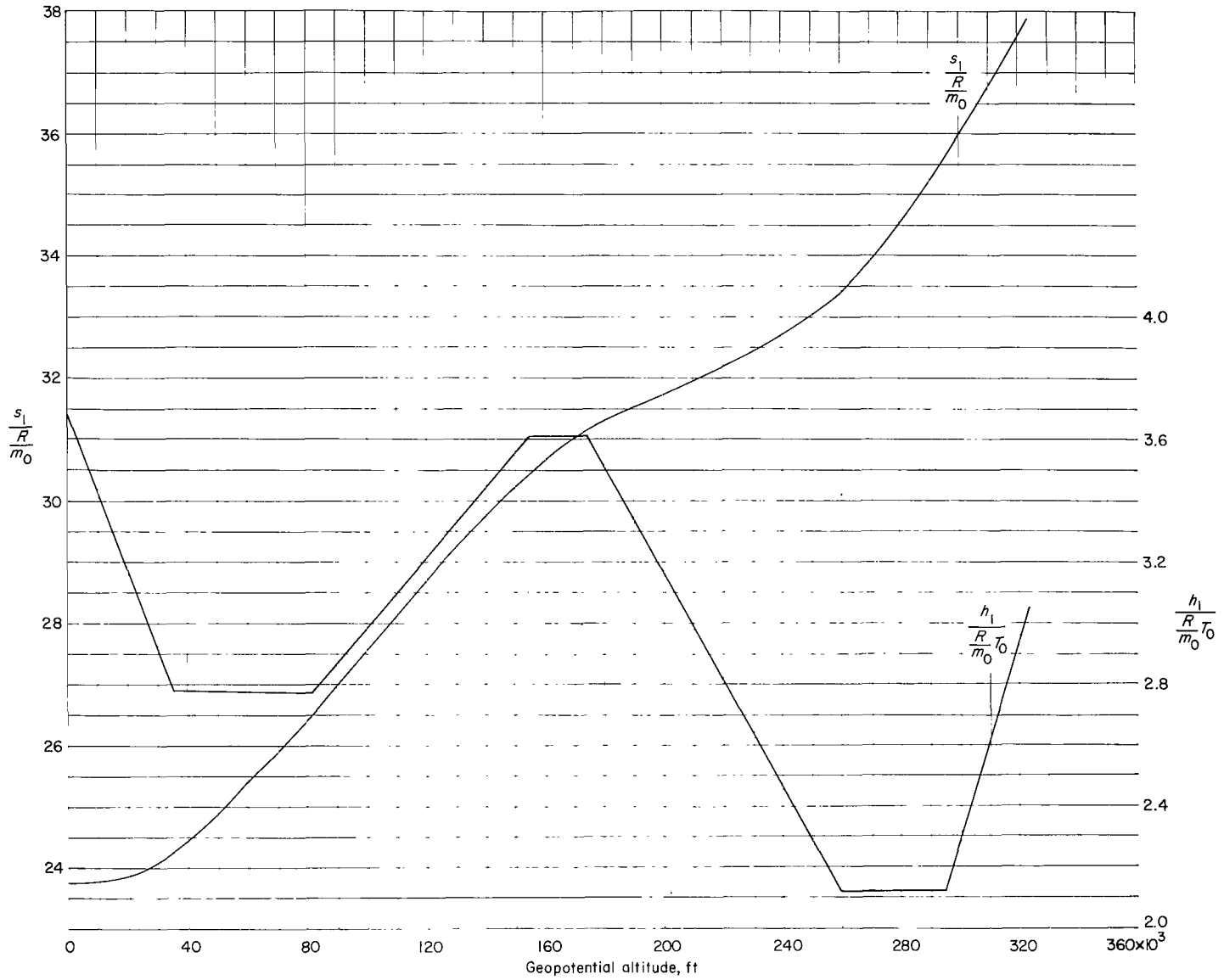
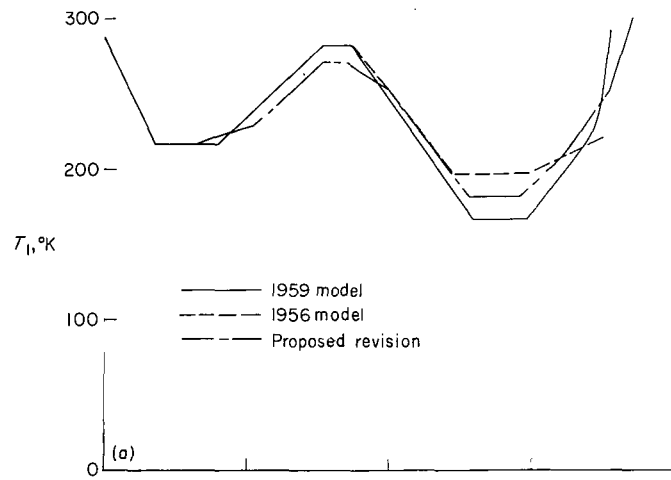
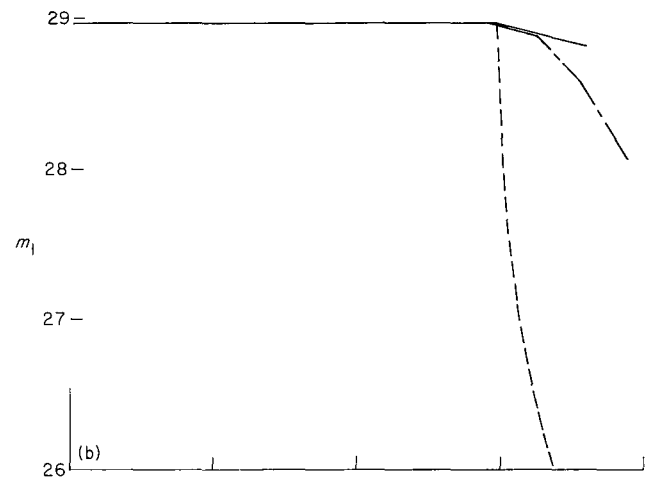


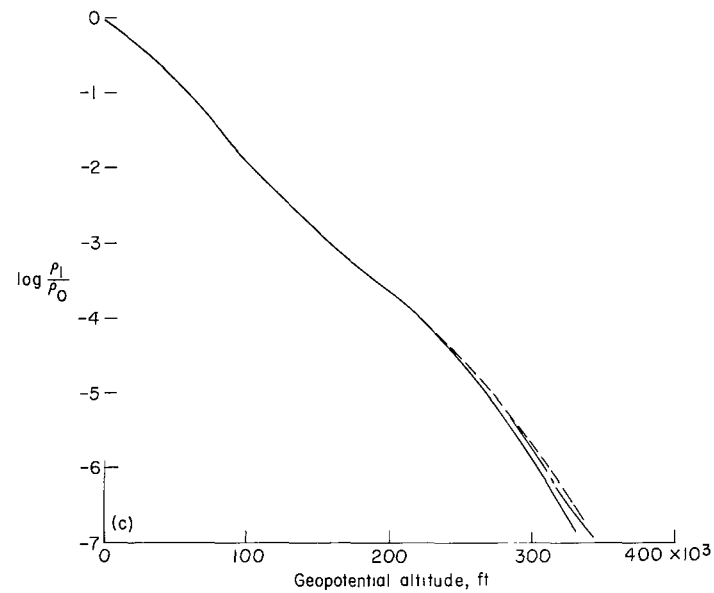
Figure 4.- Variation of ambient entropy and enthalpy with altitude.



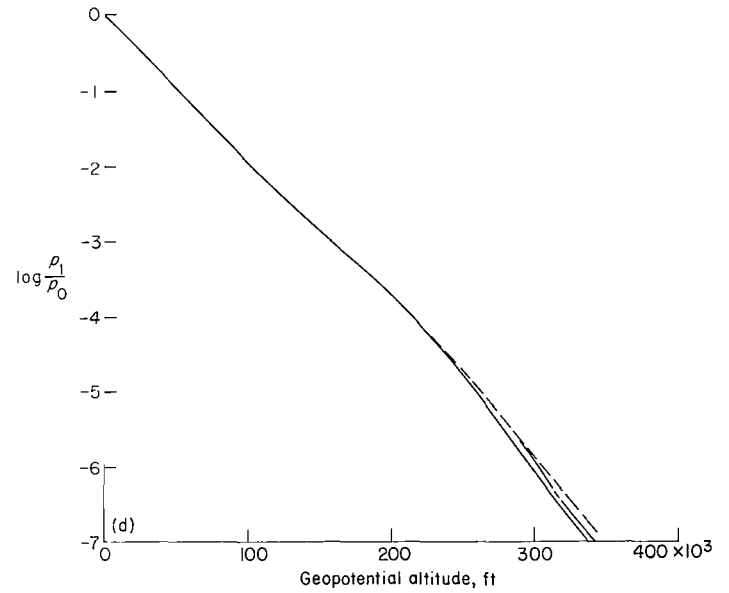
(a) Temperature.



(b) Molecular weight.

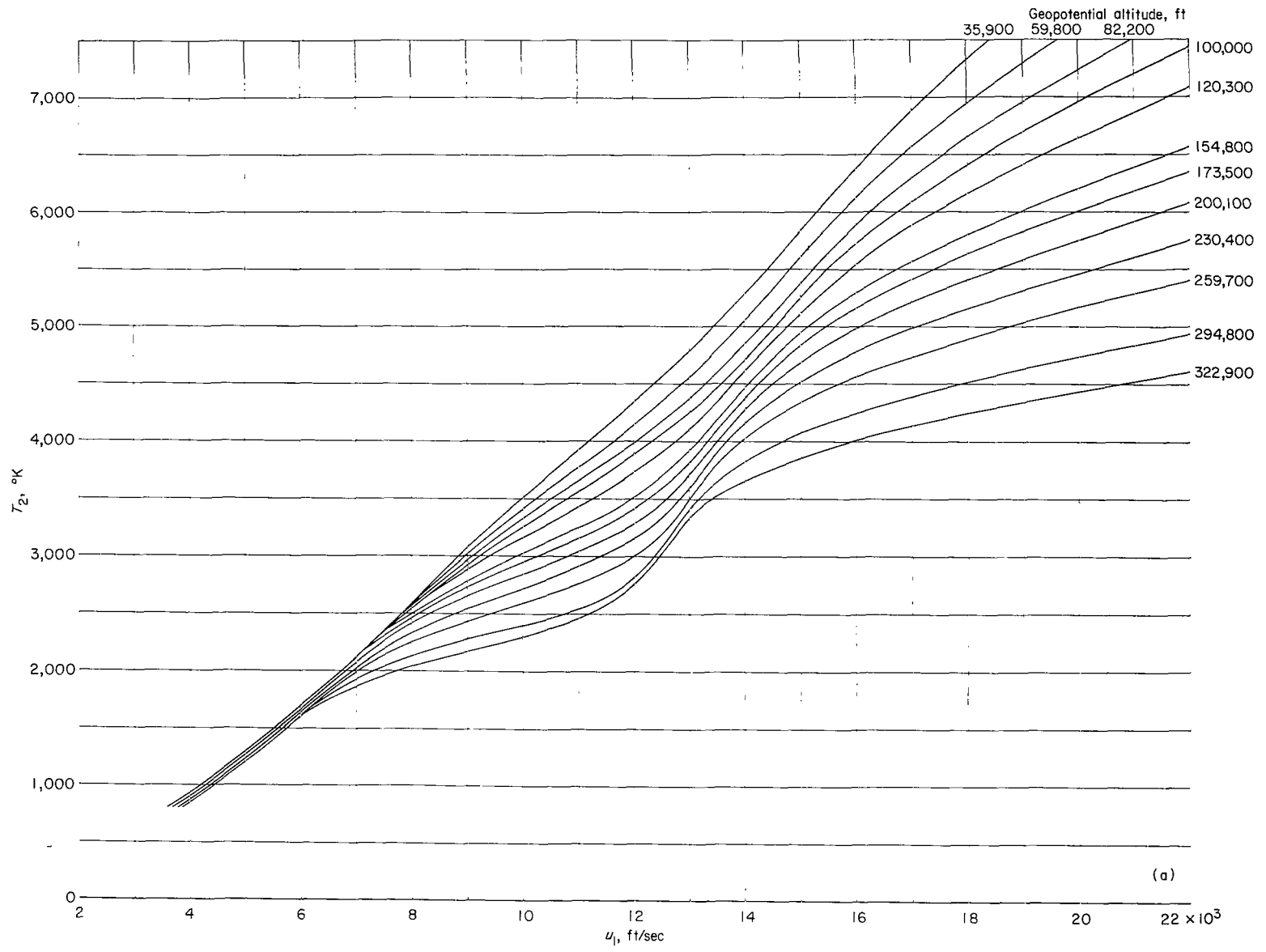


(c) Density.



(d) Pressure.

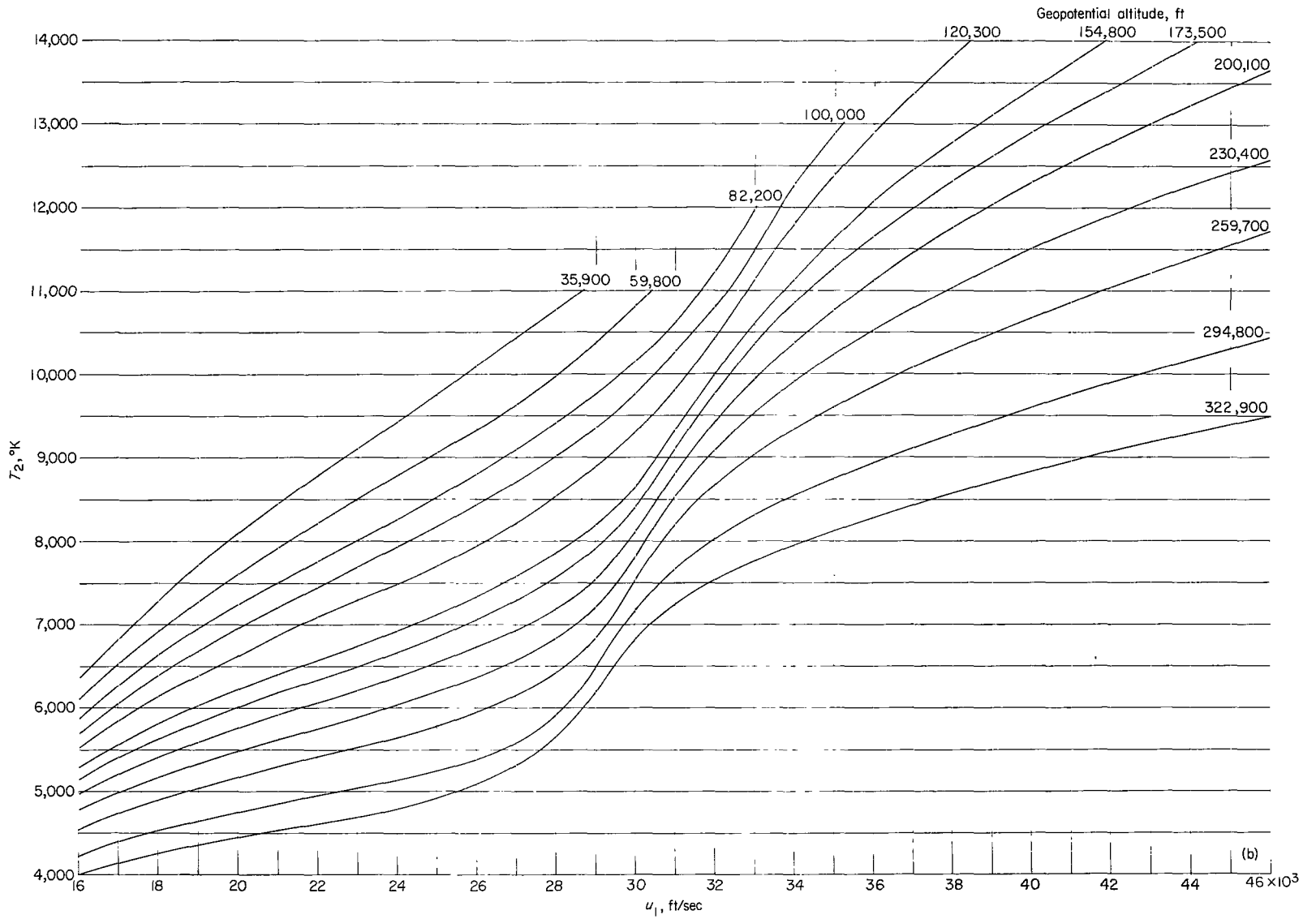
Figure 5.- Comparison of ambient air properties for the 1959 ARDC model atmosphere with the 1956 ARDC model atmosphere.



(a)

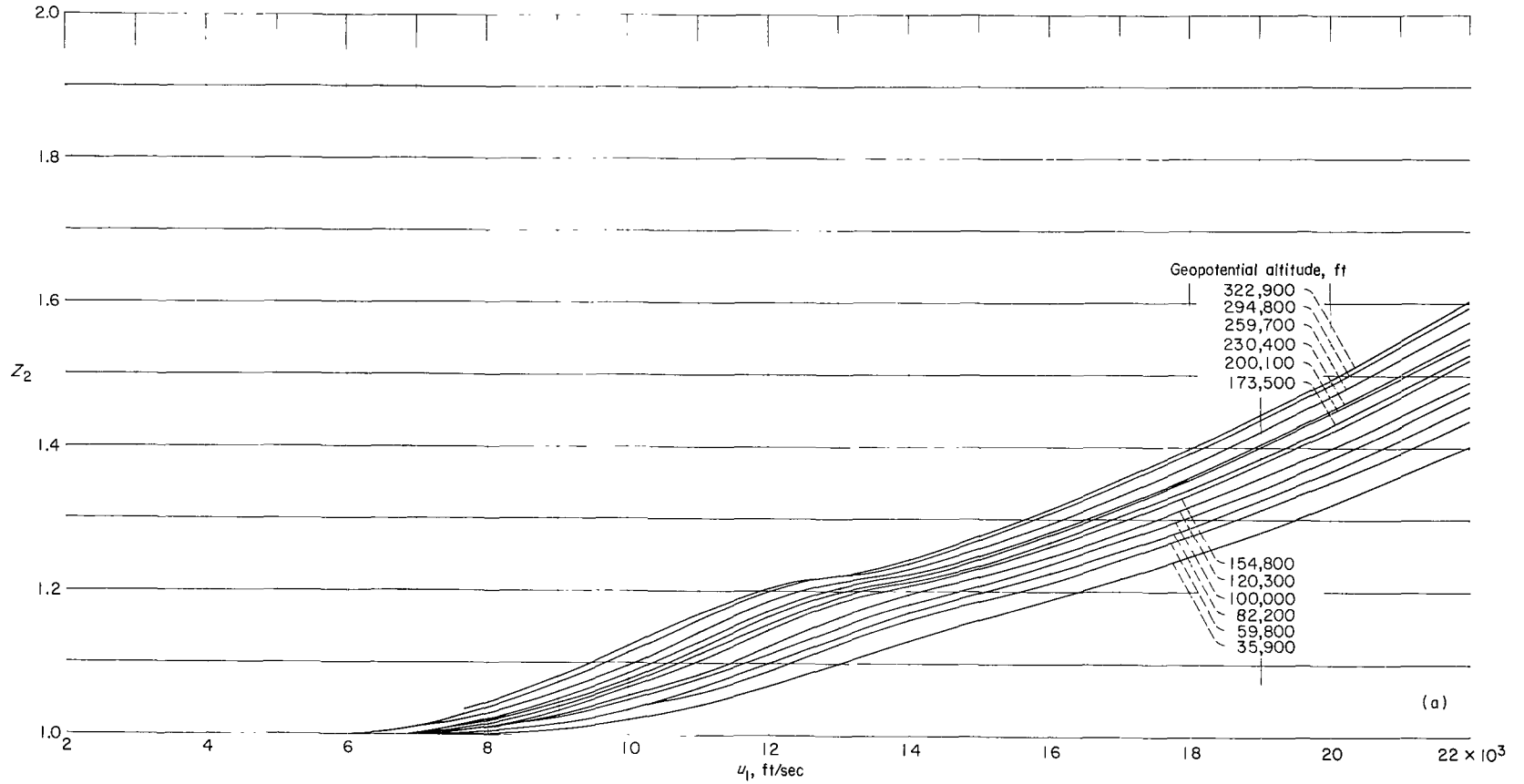
(a) Subsatellite velocity range.

Figure 6.- Variation of normal-shock temperature with velocity and altitude.



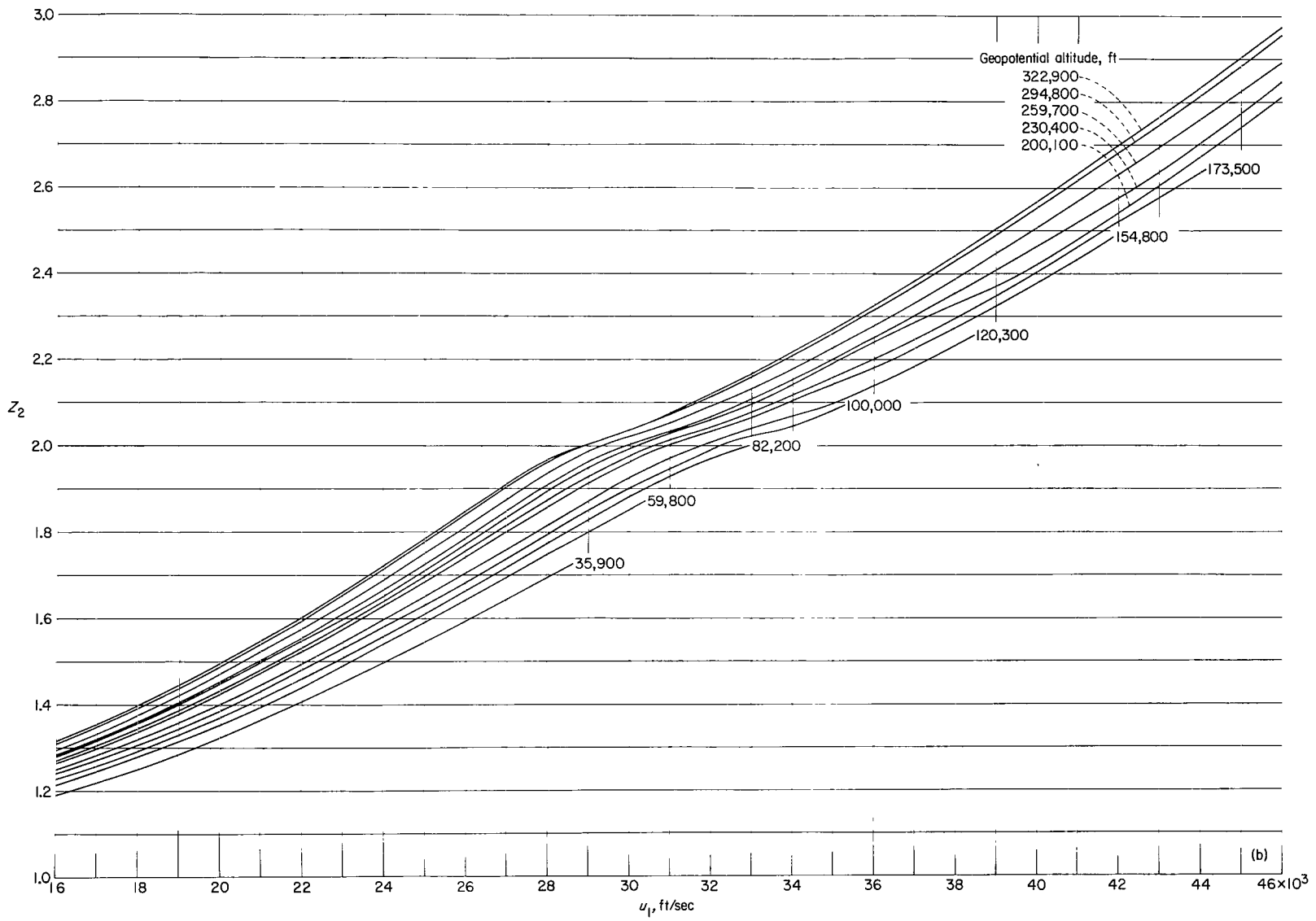
(b) Supersatellite velocity range.

Figure 6.- Concluded.



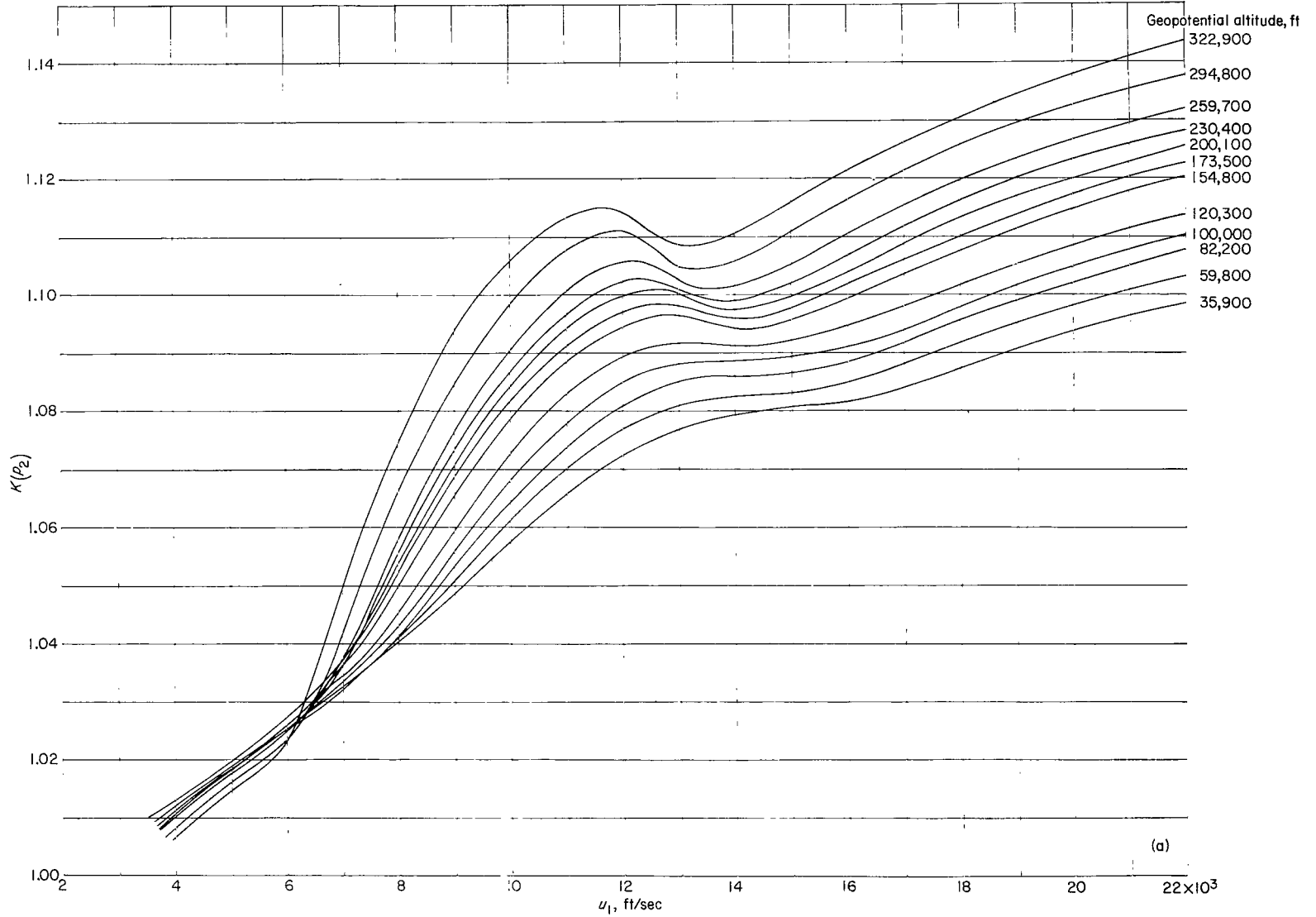
(a) Subsatellite velocity range.

Figure 7.- Variation of normal-shock compressibility factor with velocity and altitude.



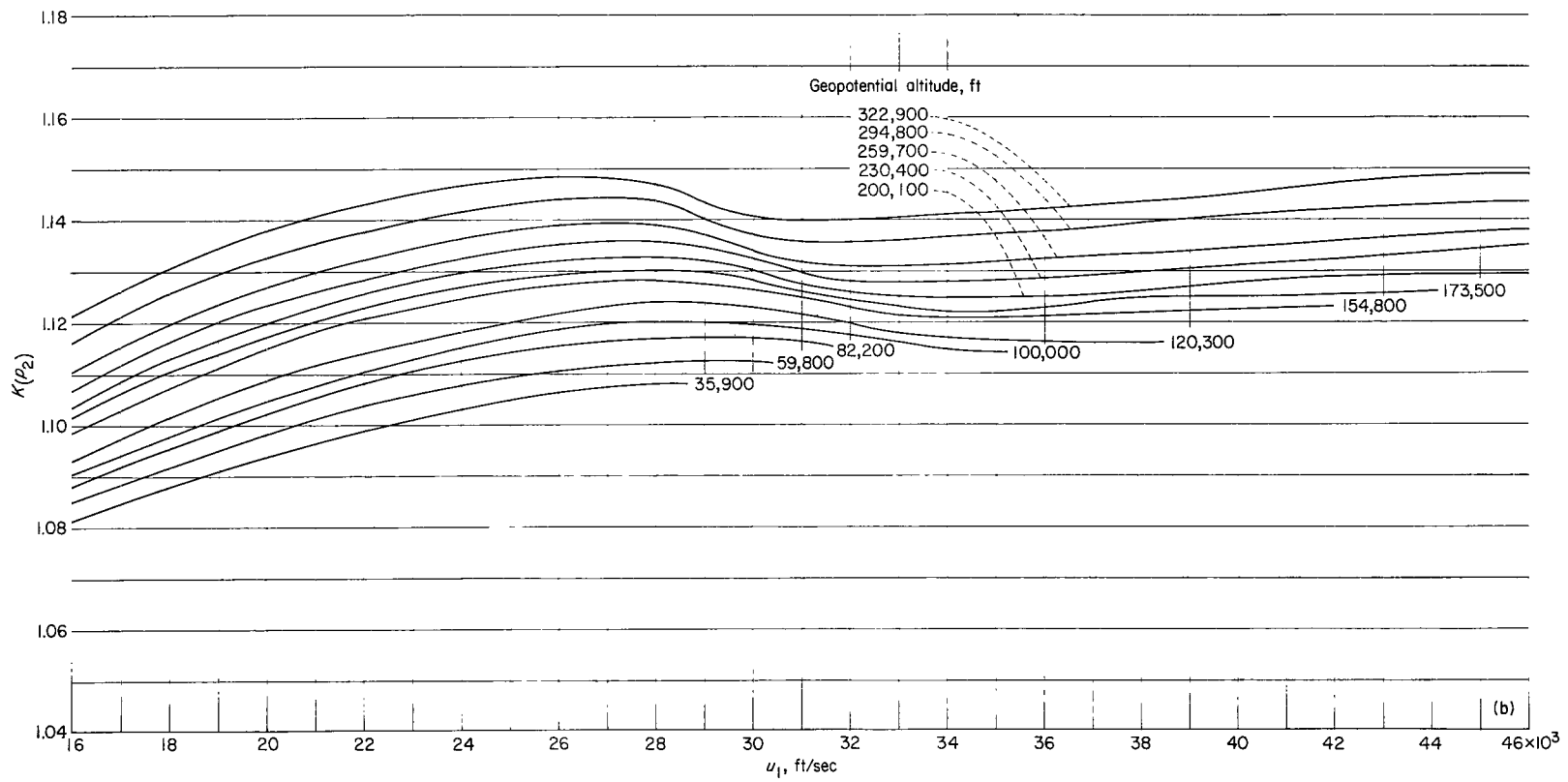
(b) Supersatellite velocity range.

Figure 7.- Concluded.



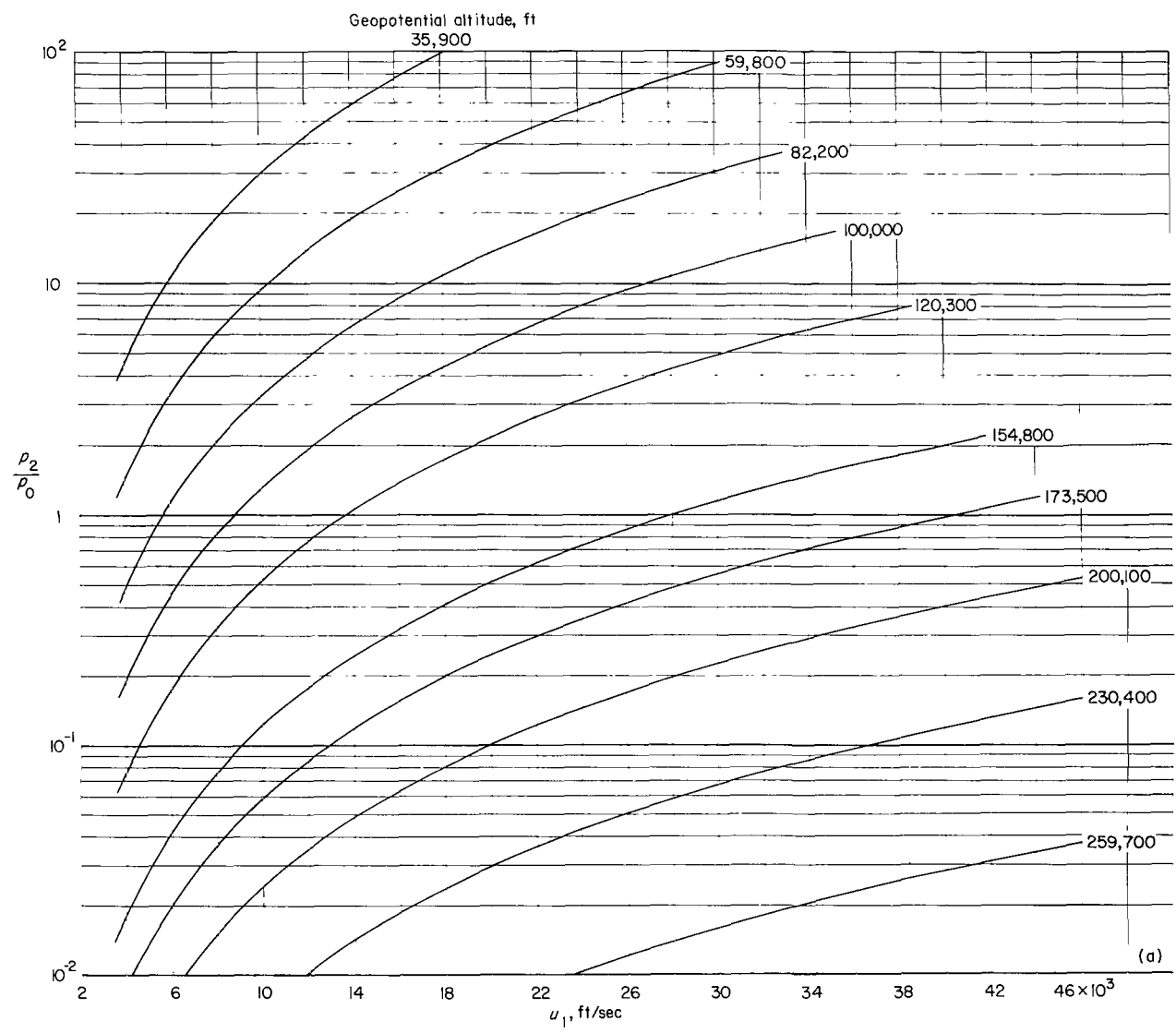
(a) Subsatellite velocity range.

Figure 8.- Variation of normal-shock real-to-ideal pressure ratio with velocity and altitude.



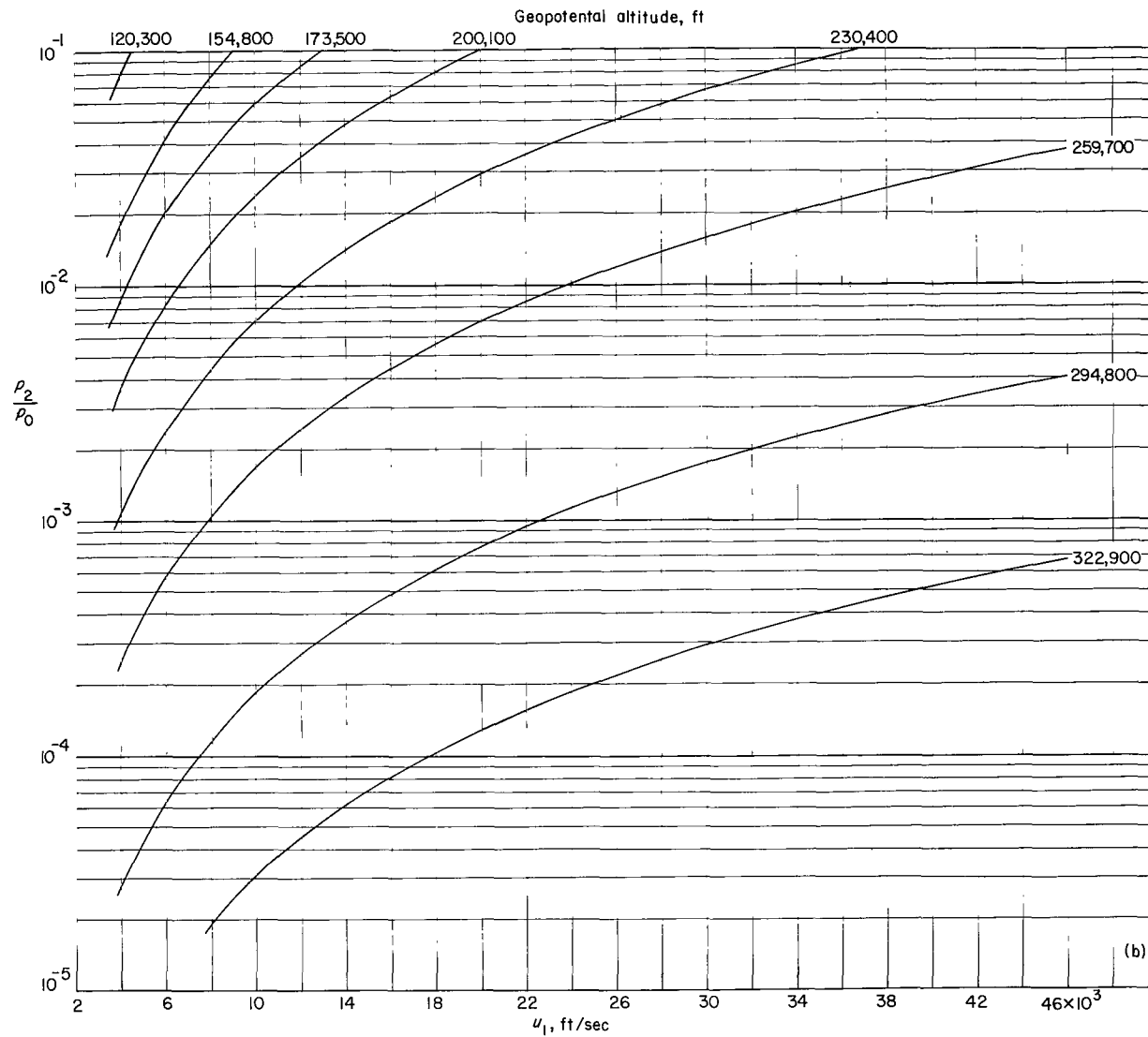
(b) Supersatellite velocity range.

Figure 8.- Concluded.



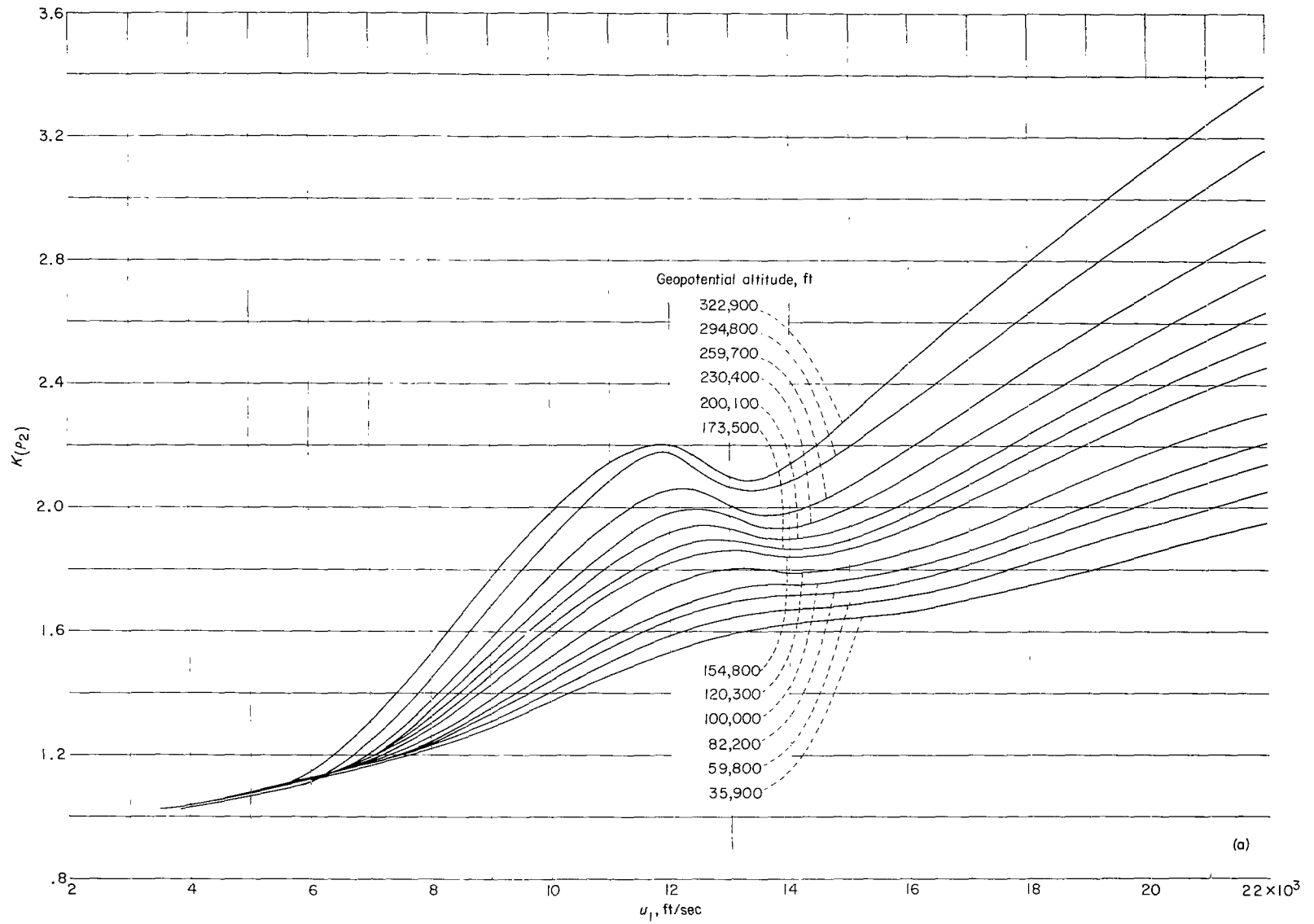
(a) Stratospheric altitude range.

Figure 9.- Variation of normalized normal-shock pressure with velocity and altitude.



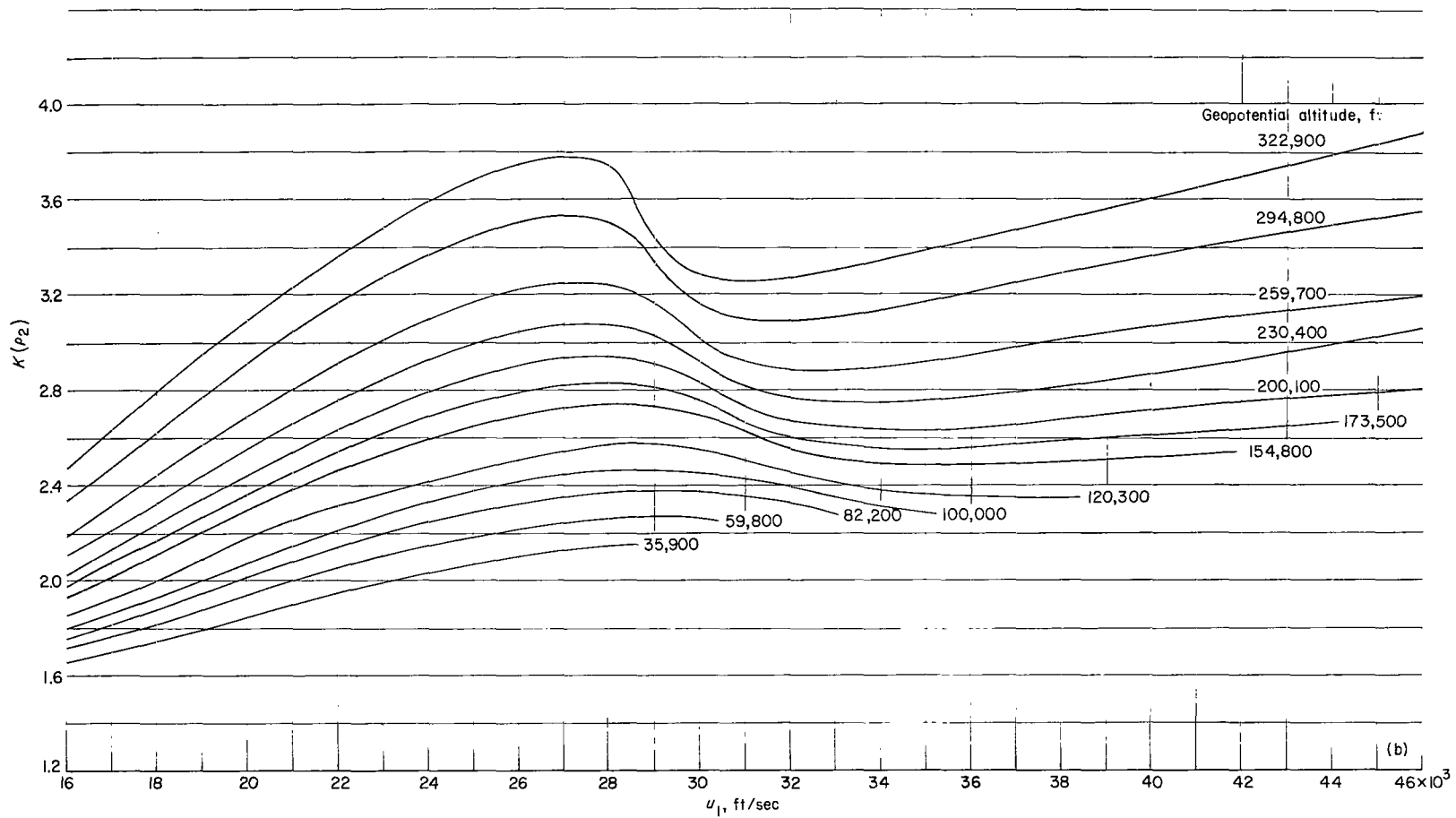
(b) Mesospheric altitude range.

Figure 9.- Concluded.



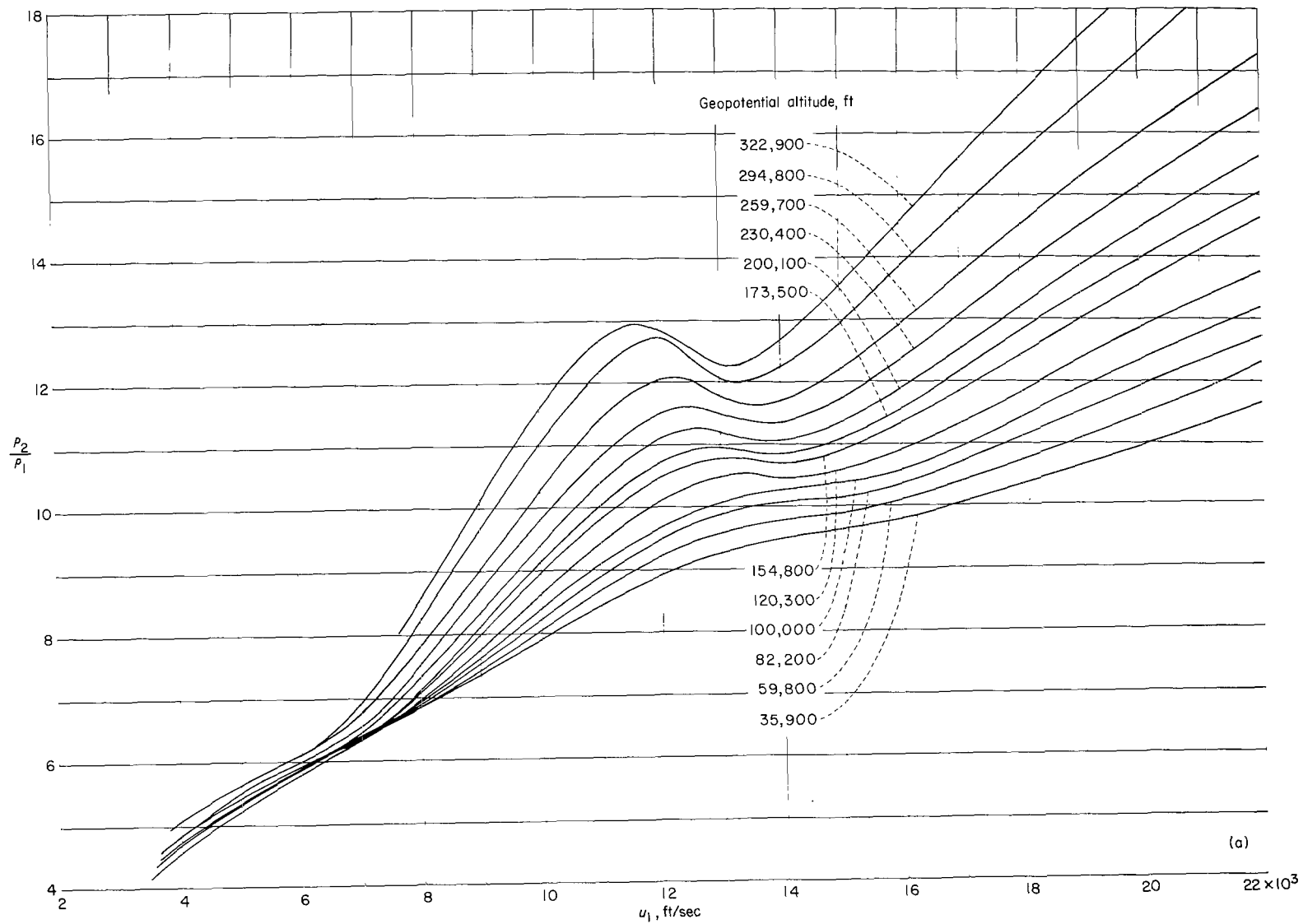
(a) Subsatellite velocity range.

Figure 10.- Variation of normal-shock real-to-ideal density ratio with velocity and altitude.



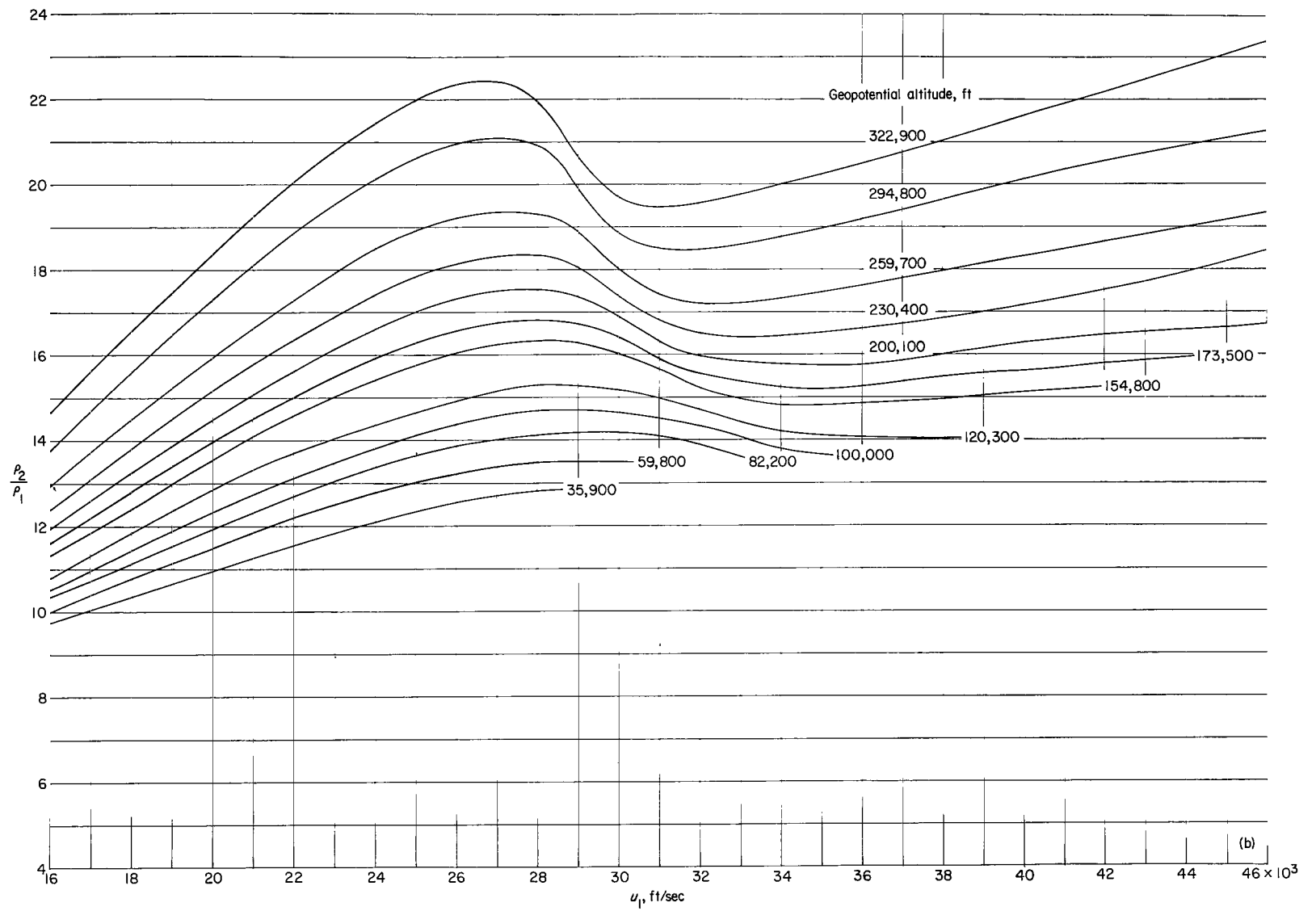
(b) Supersatellite velocity range.

Figure 10.- Concluded.



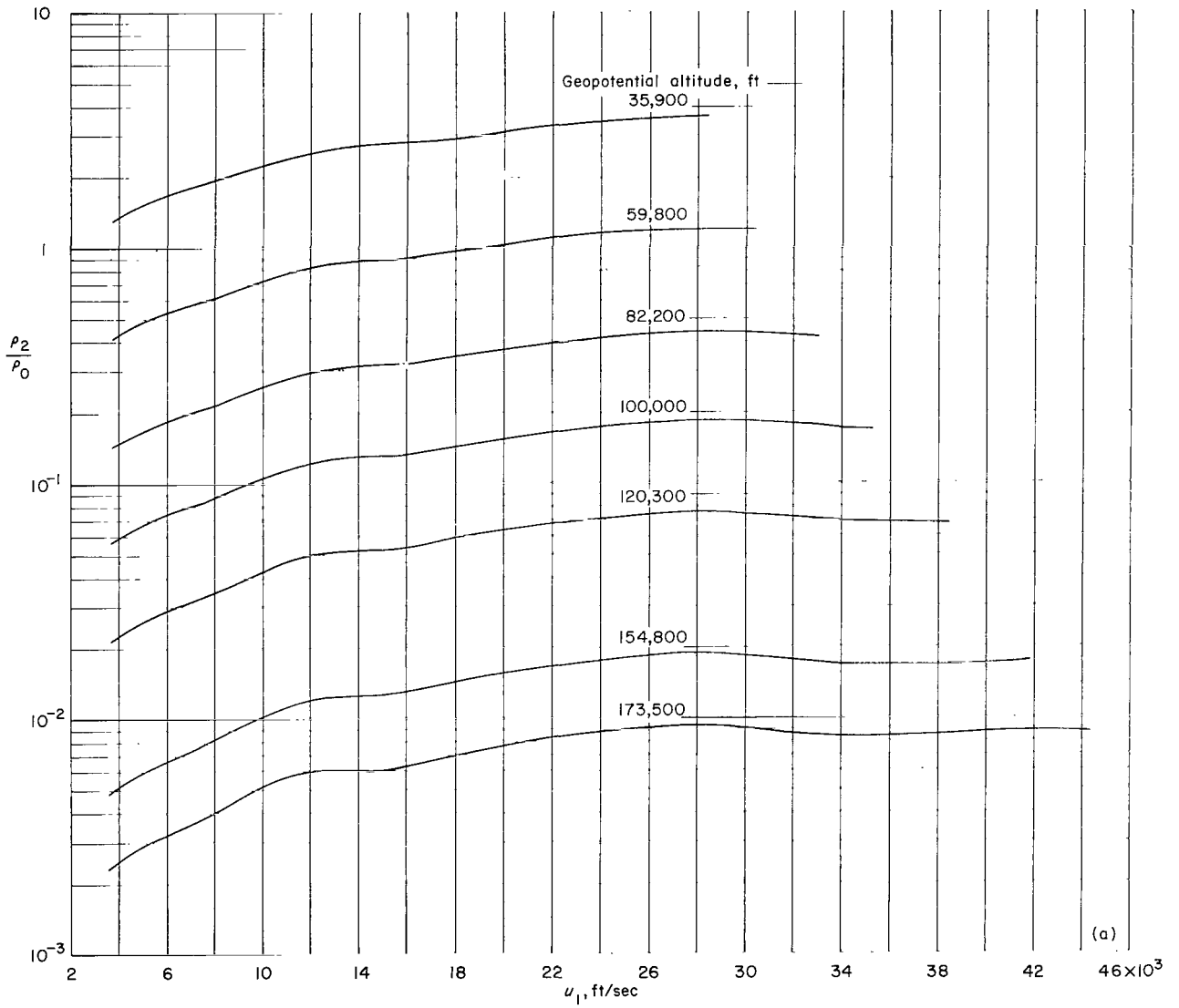
(a) Subsatellite velocity range.

Figure 11.- Variation of normal-shock density ratio with velocity and altitude.



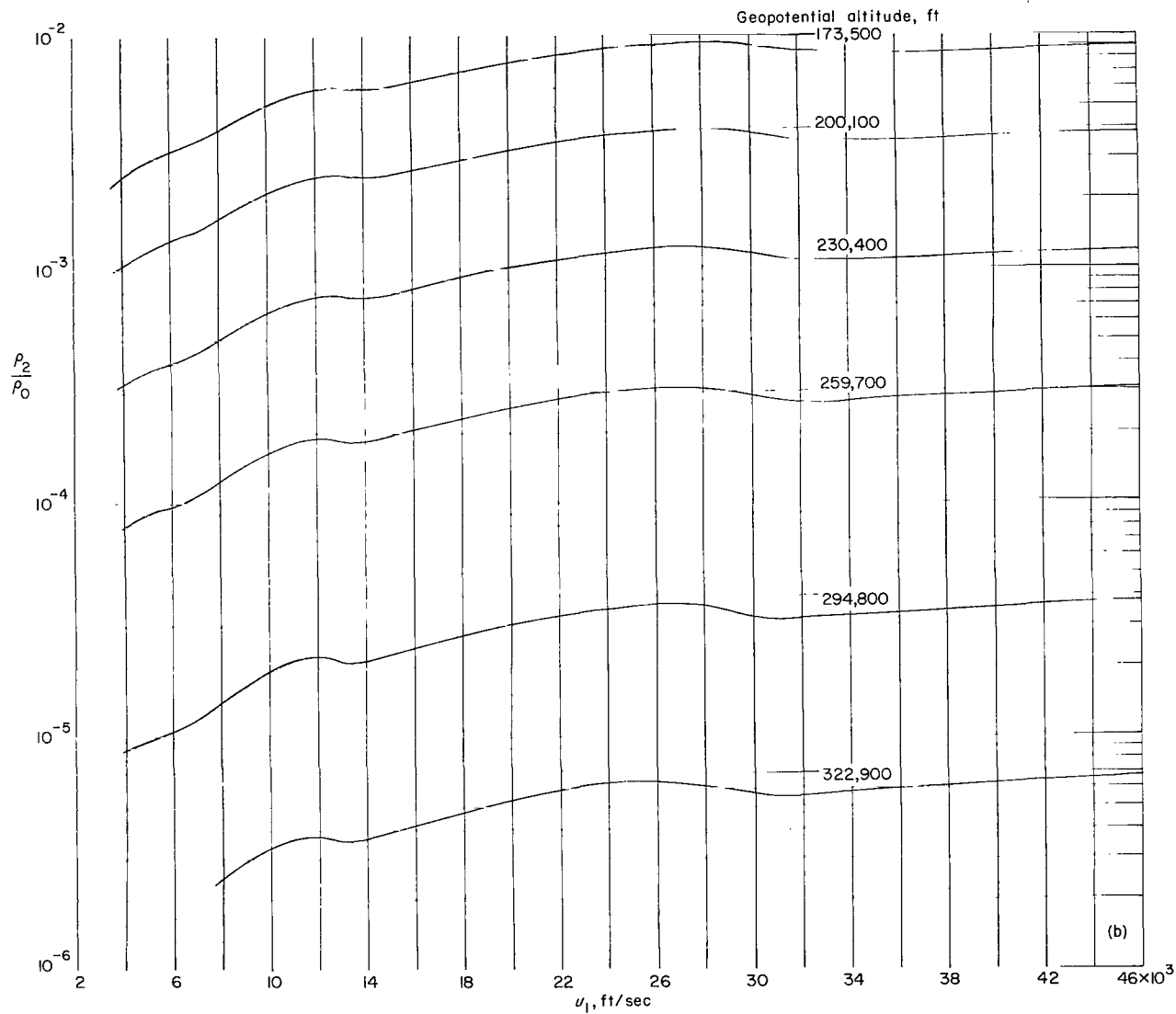
(b) Supersatellite velocity range.

Figure 11.- Concluded.



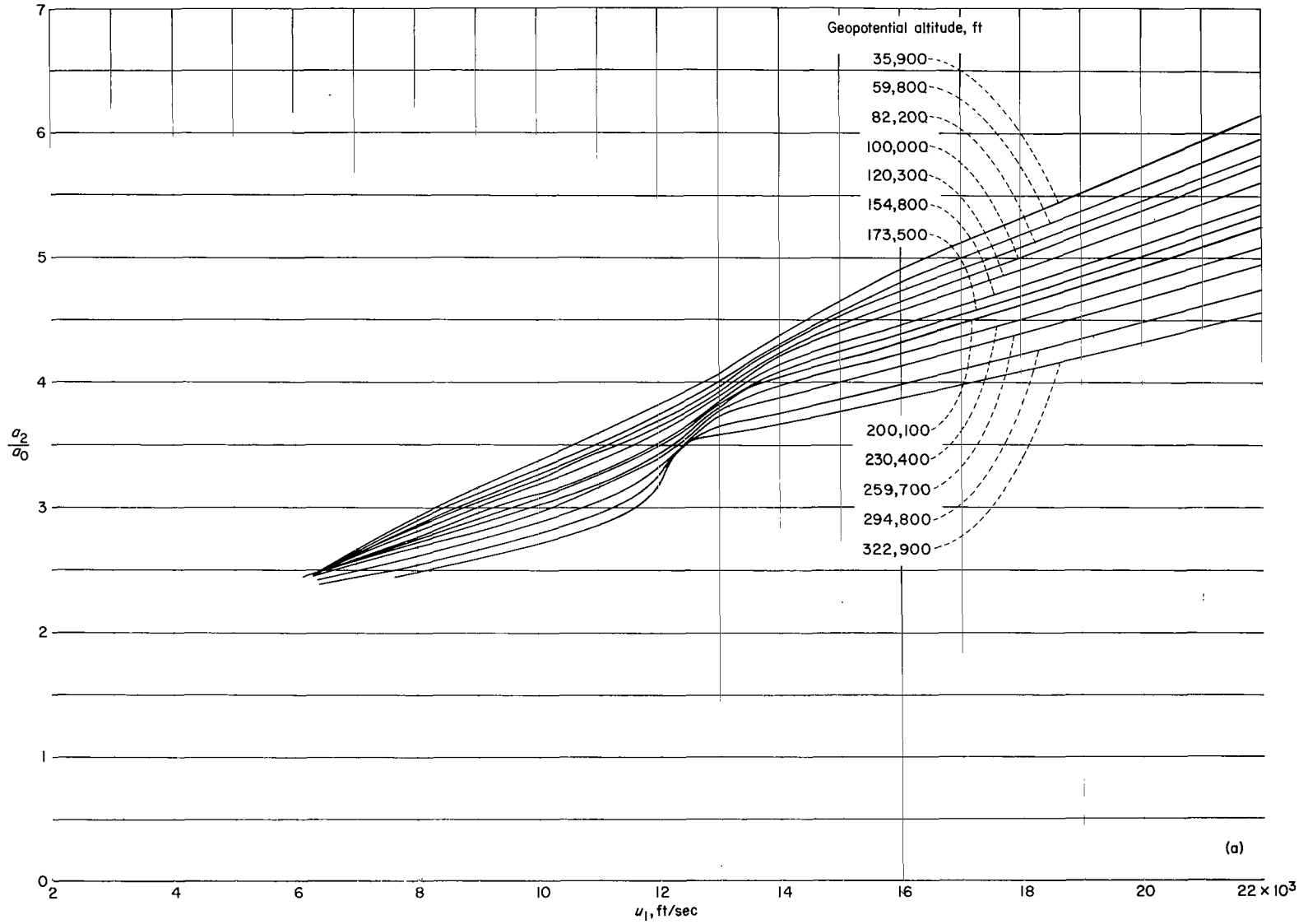
(a) Stratospheric altitude range.

Figure 12.- Variation of normalized normal-shock density with velocity and altitude.



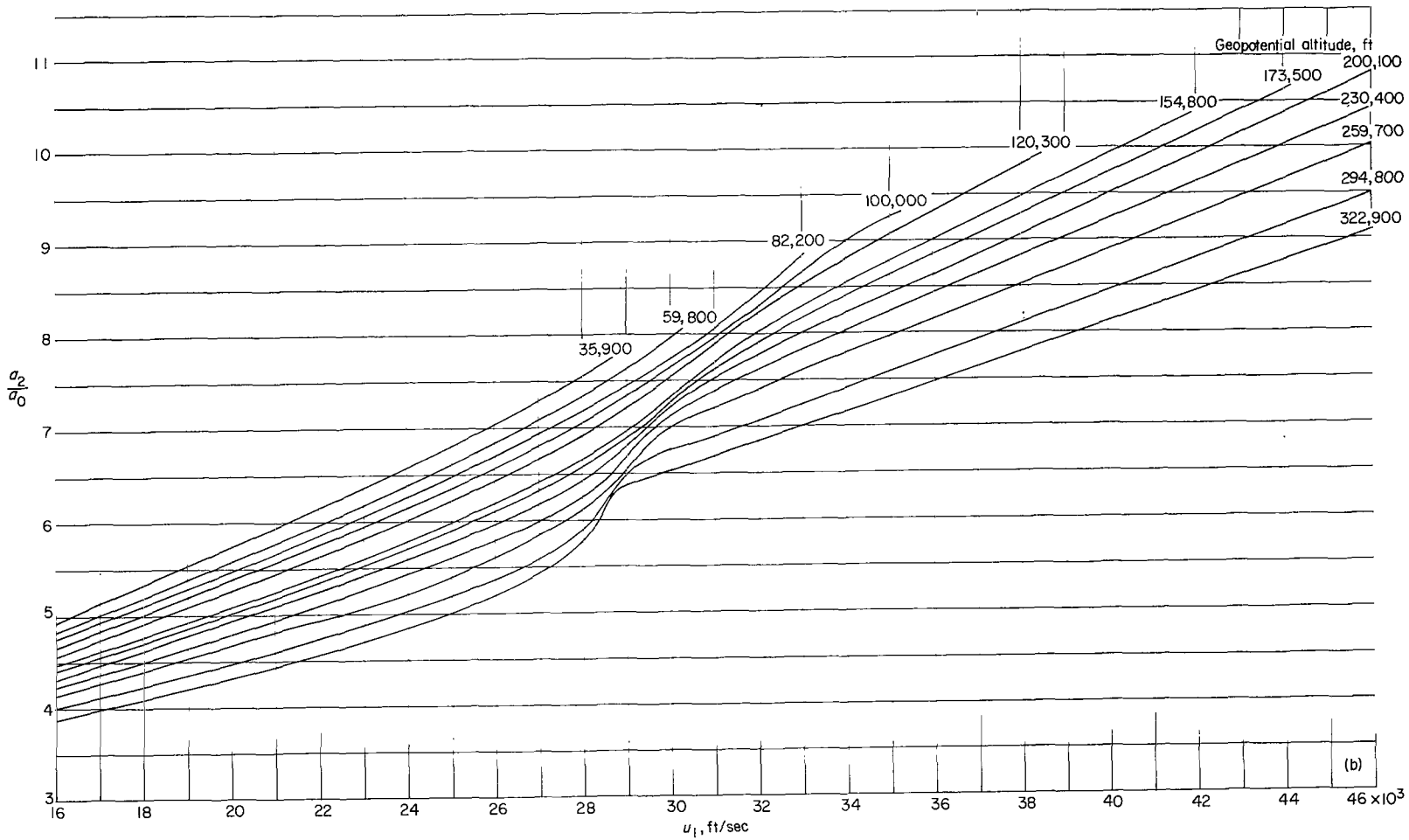
(b) Mesospheric altitude range.

Figure 12.- Concluded.



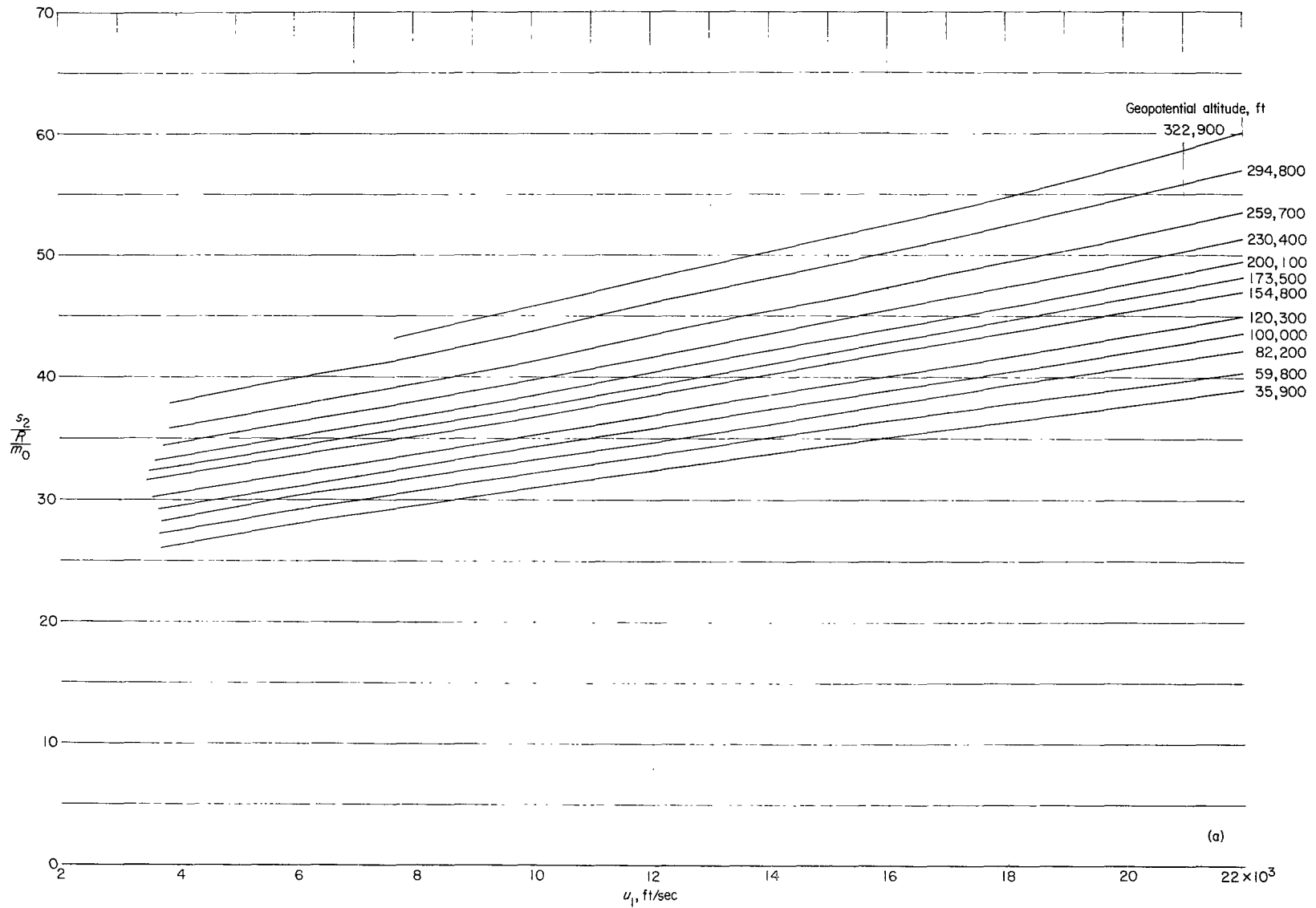
(a) Subsatellite velocity range.

Figure 13.- Variation of normalized normal-shock velocity of sound with velocity and altitude.



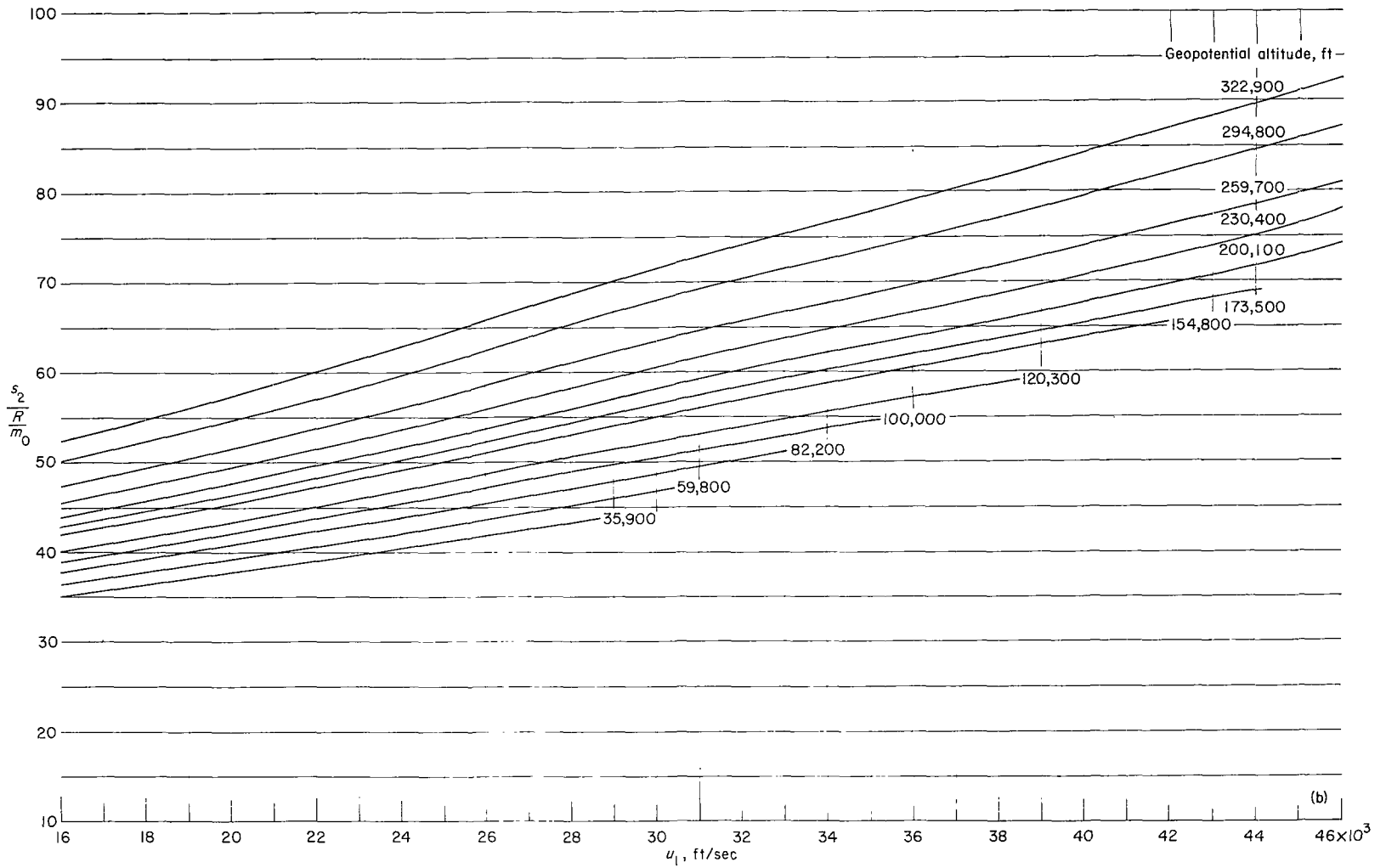
(b) Supersatellite velocity range.

Figure 13.- Concluded.



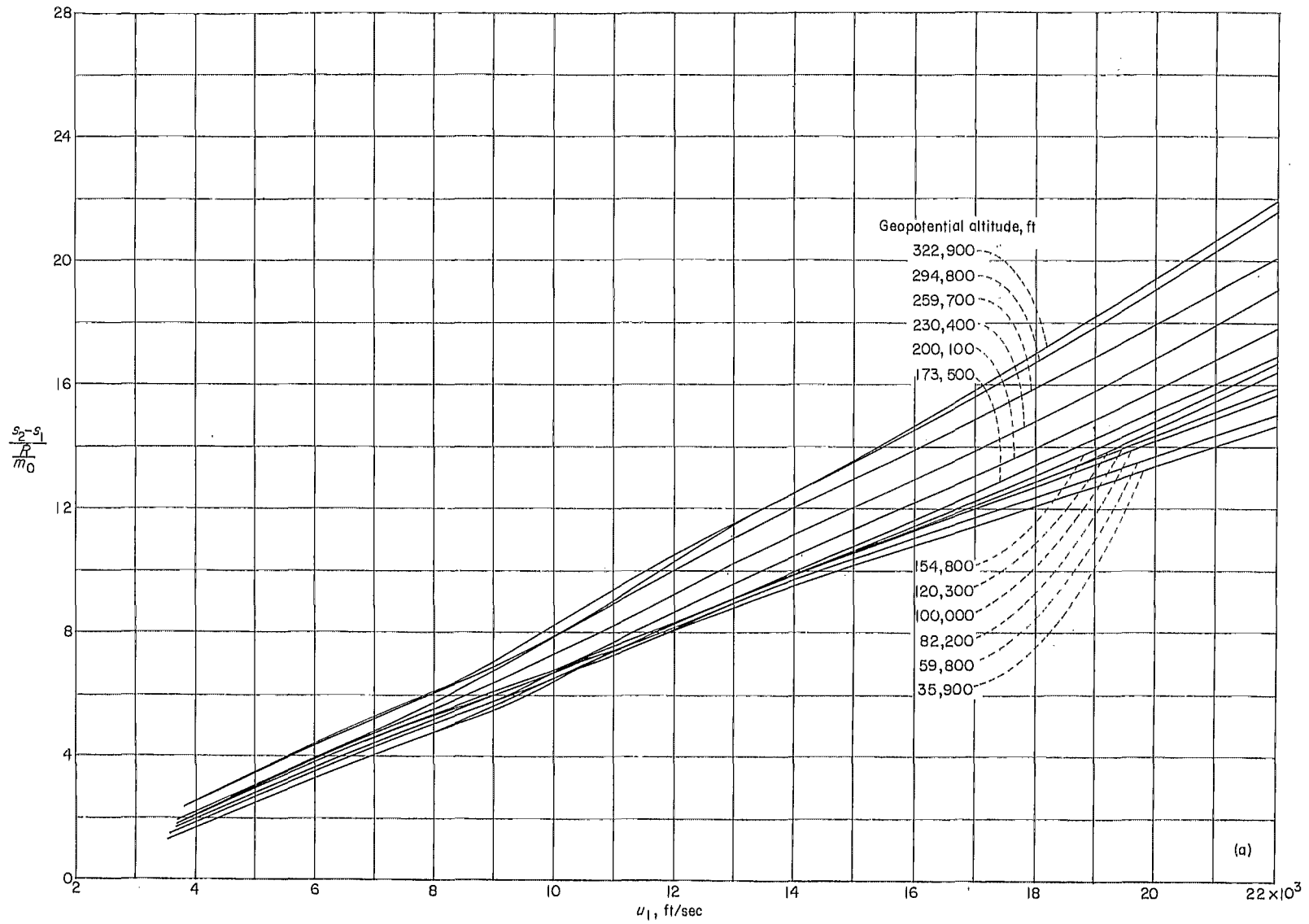
(a) Subsatellite velocity range.

Figure 14.- Variation of normal-shock entropy with velocity and altitude.



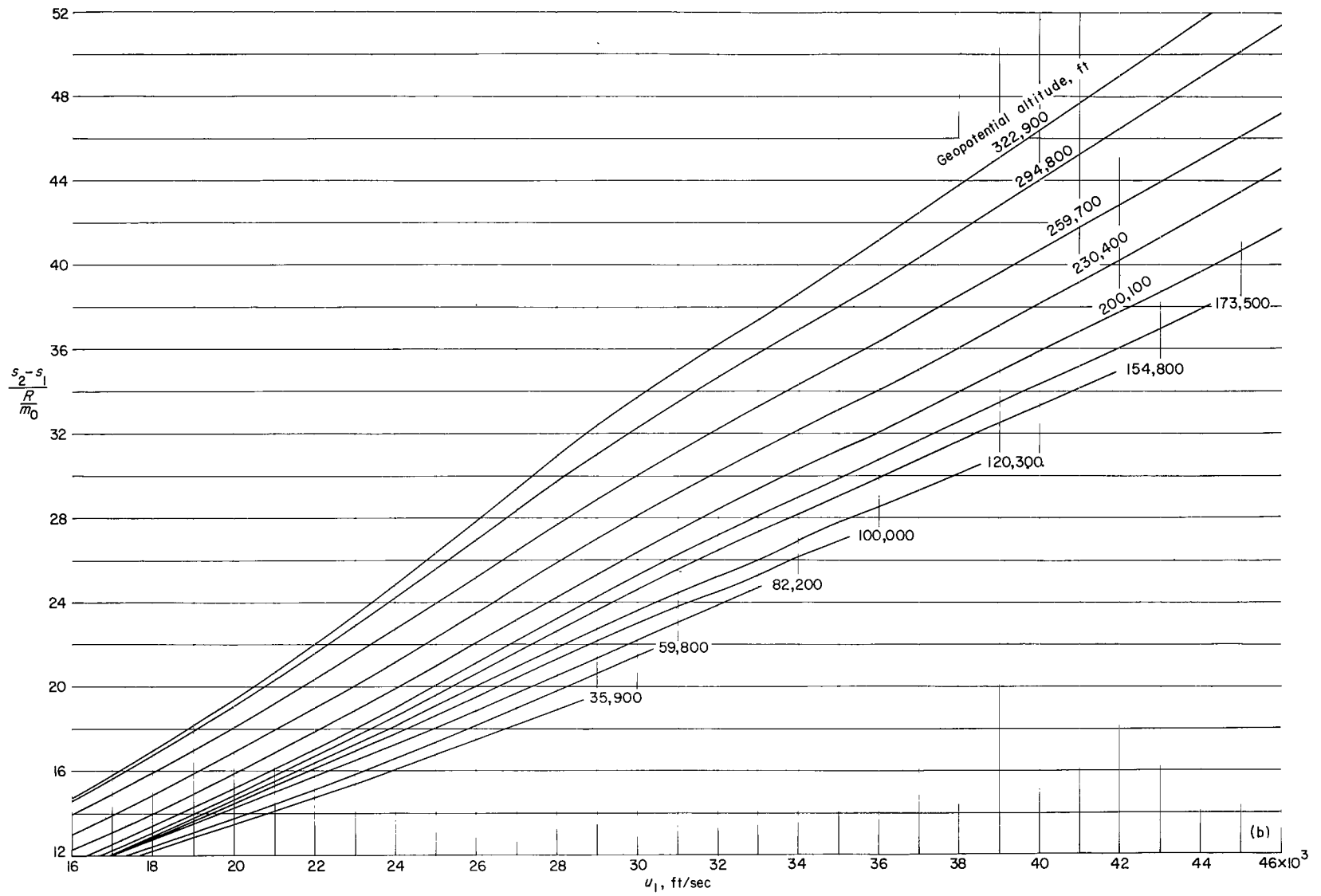
(b) Supersatellite velocity range.

Figure 14.- Concluded.



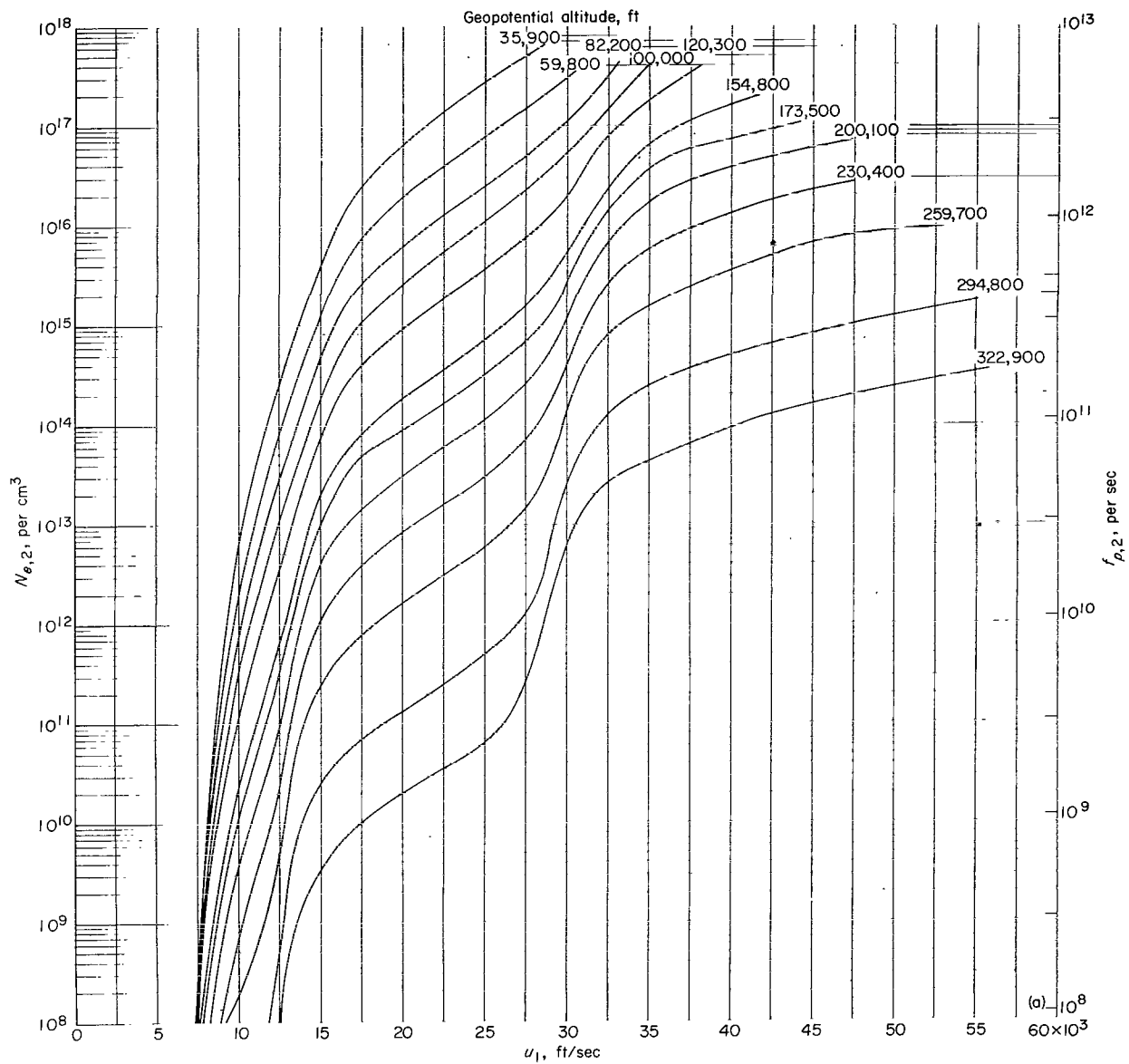
(a) Subsatellite velocity range.

Figure 15.- Variation of normal-shock entropy increase with velocity and altitude.



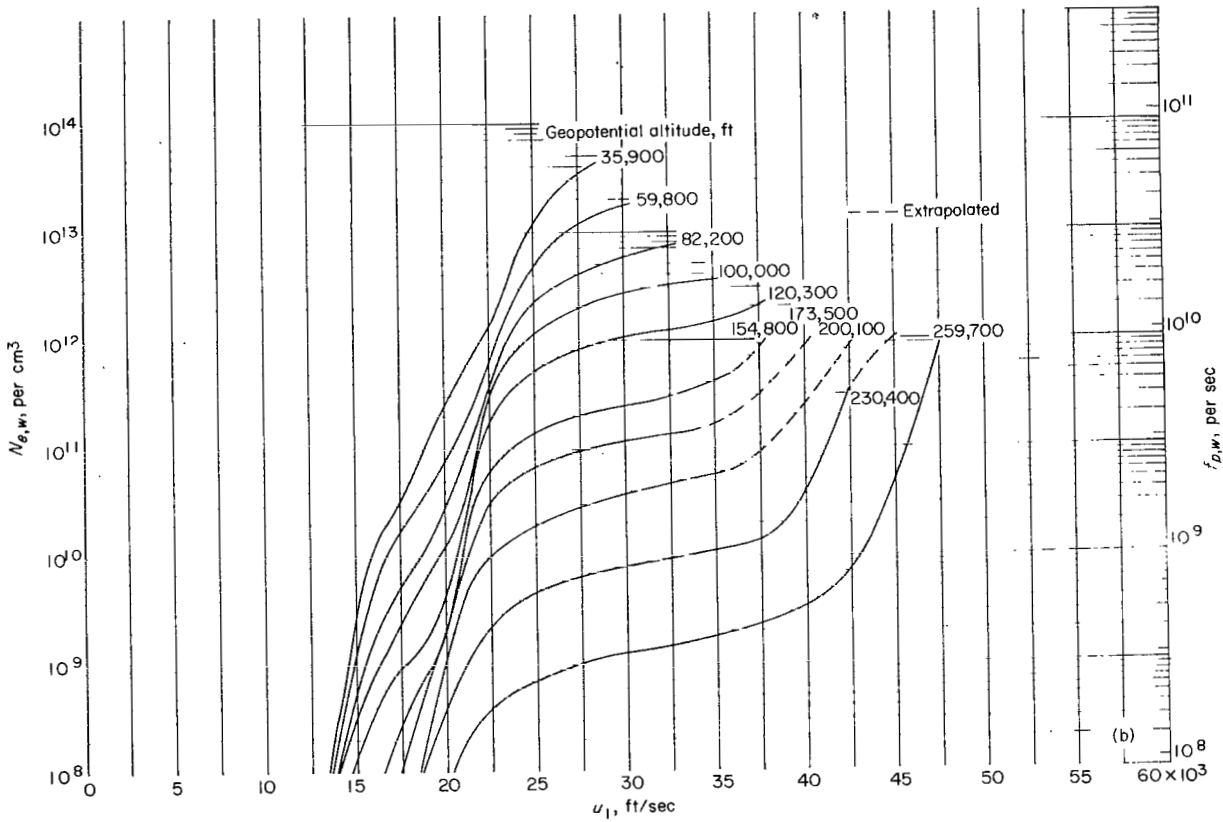
(b) Supersatellite velocity range.

Figure 15.- Concluded.



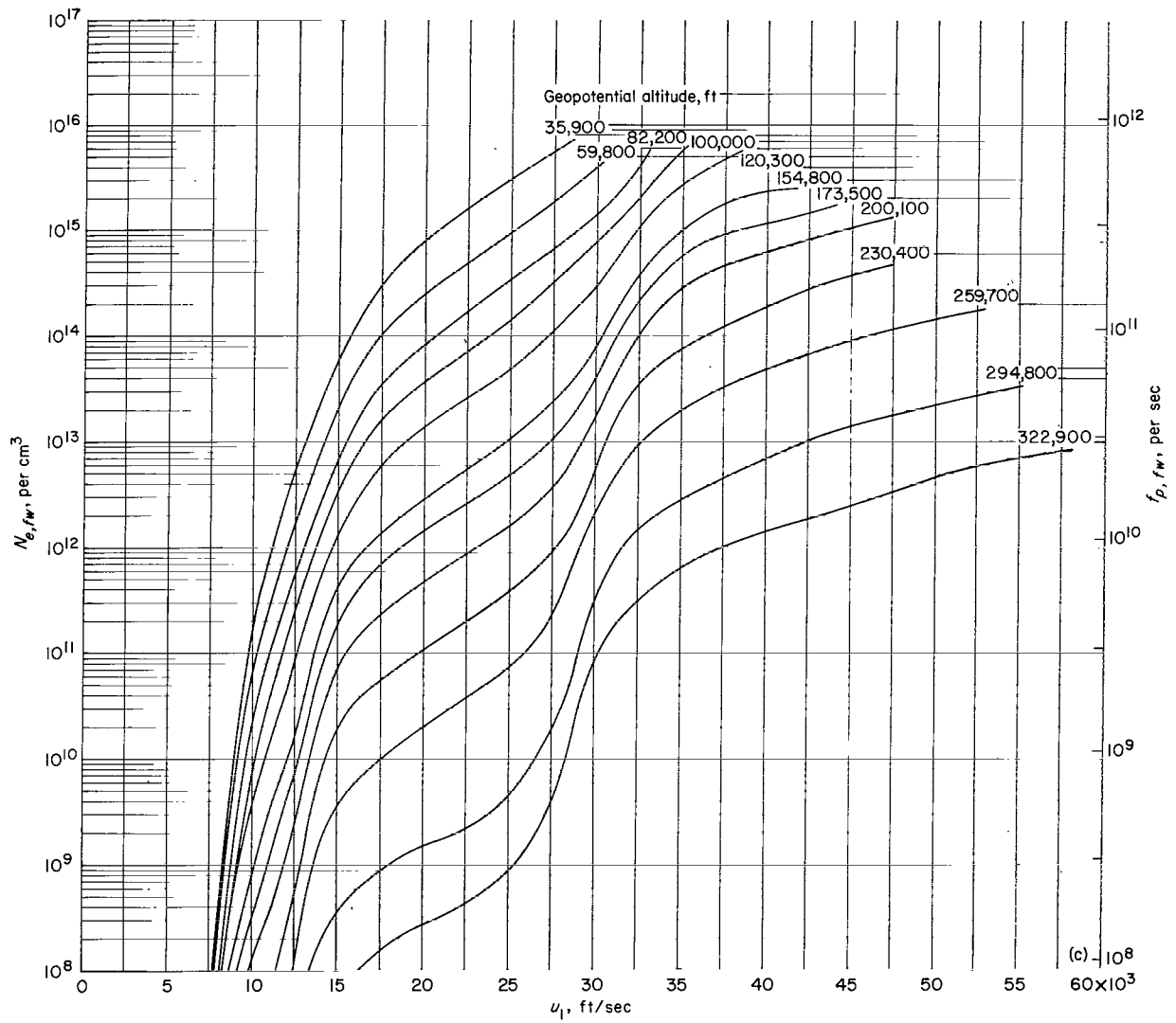
(a) Equilibrium normal-shock flow.

Figure 16.- Variation of electron concentration with velocity and altitude.



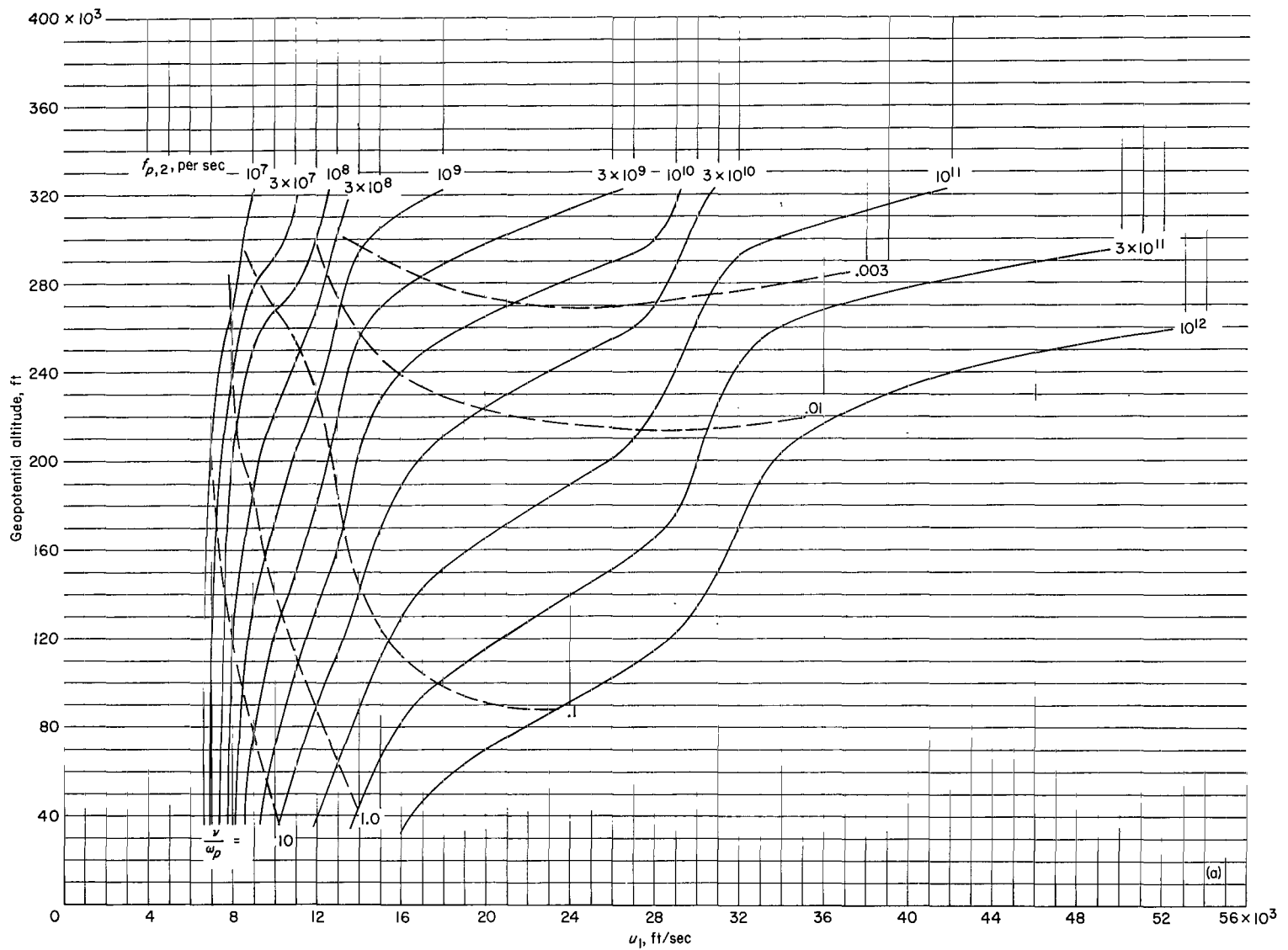
(b) Equilibrium far-wake flow.

Figure 16.- Continued.



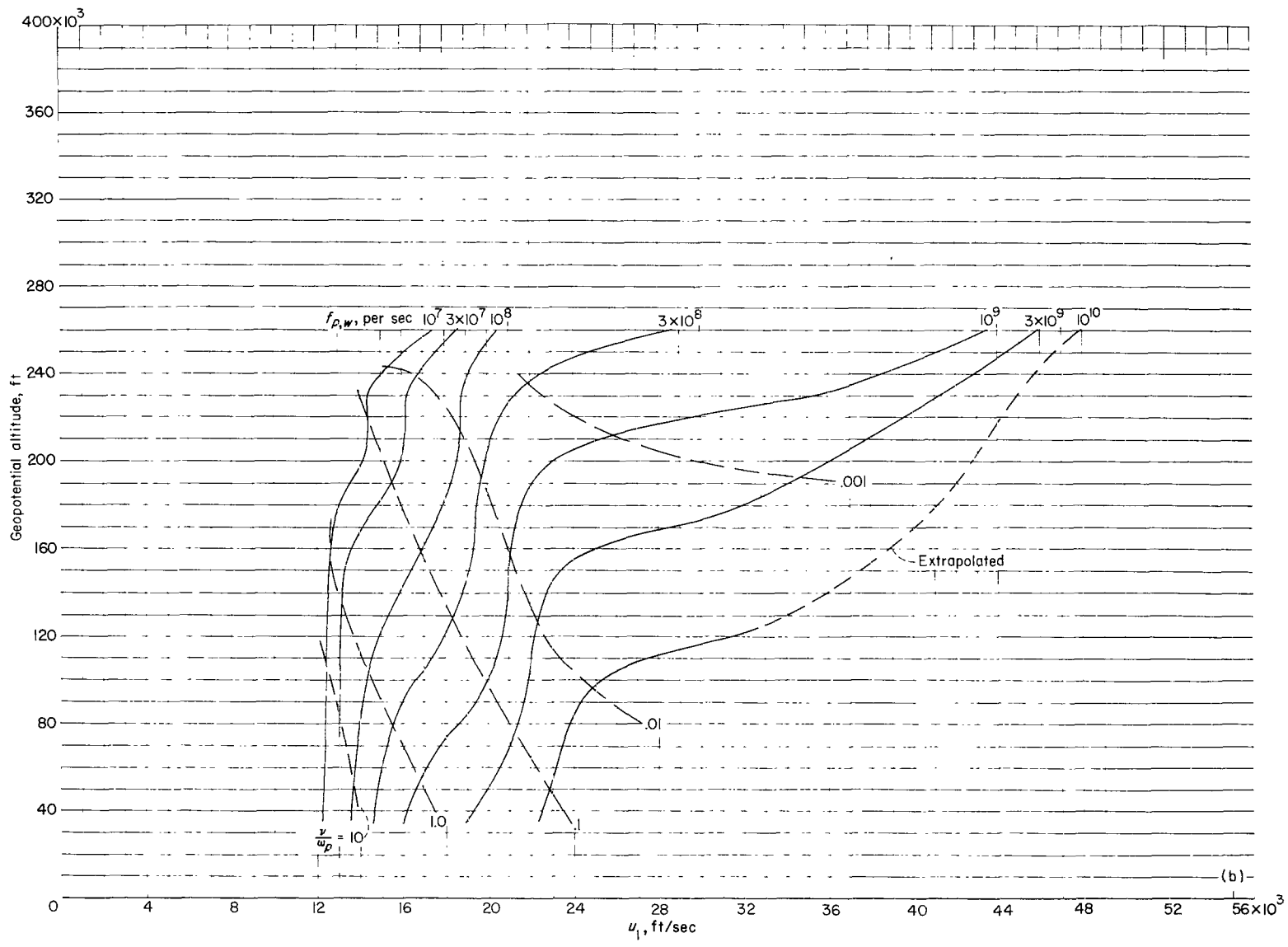
(c) Frozen far-wake flow.

Figure 16.- Concluded.



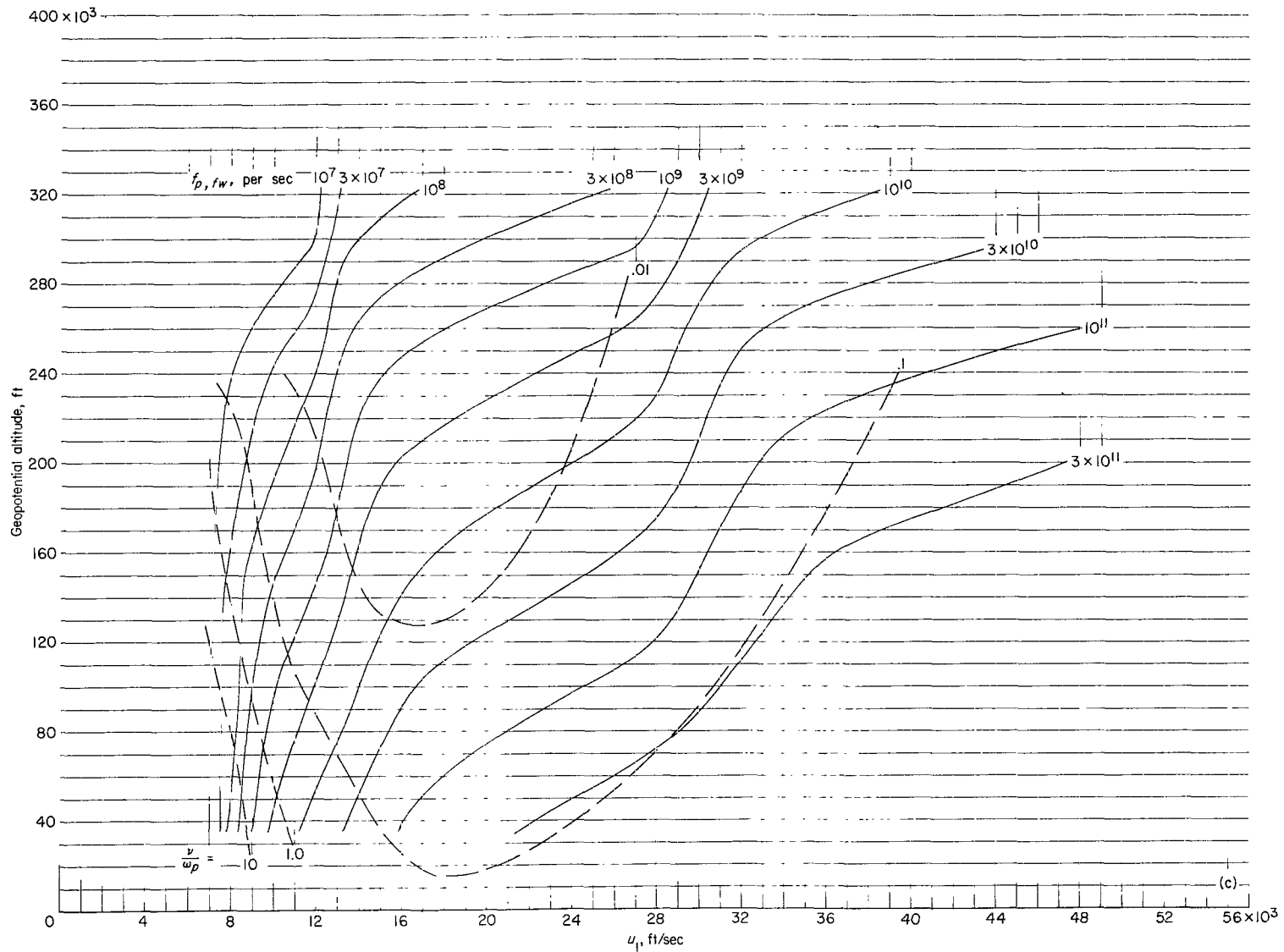
(a) Equilibrium normal-shock flow.

Figure 17.- Variation of plasma frequency with velocity and altitude.



(b) Equilibrium far-wake flow.

Figure 17.- Continued.



(c) Frozen far-wake flow.

Figure 17.- Concluded.

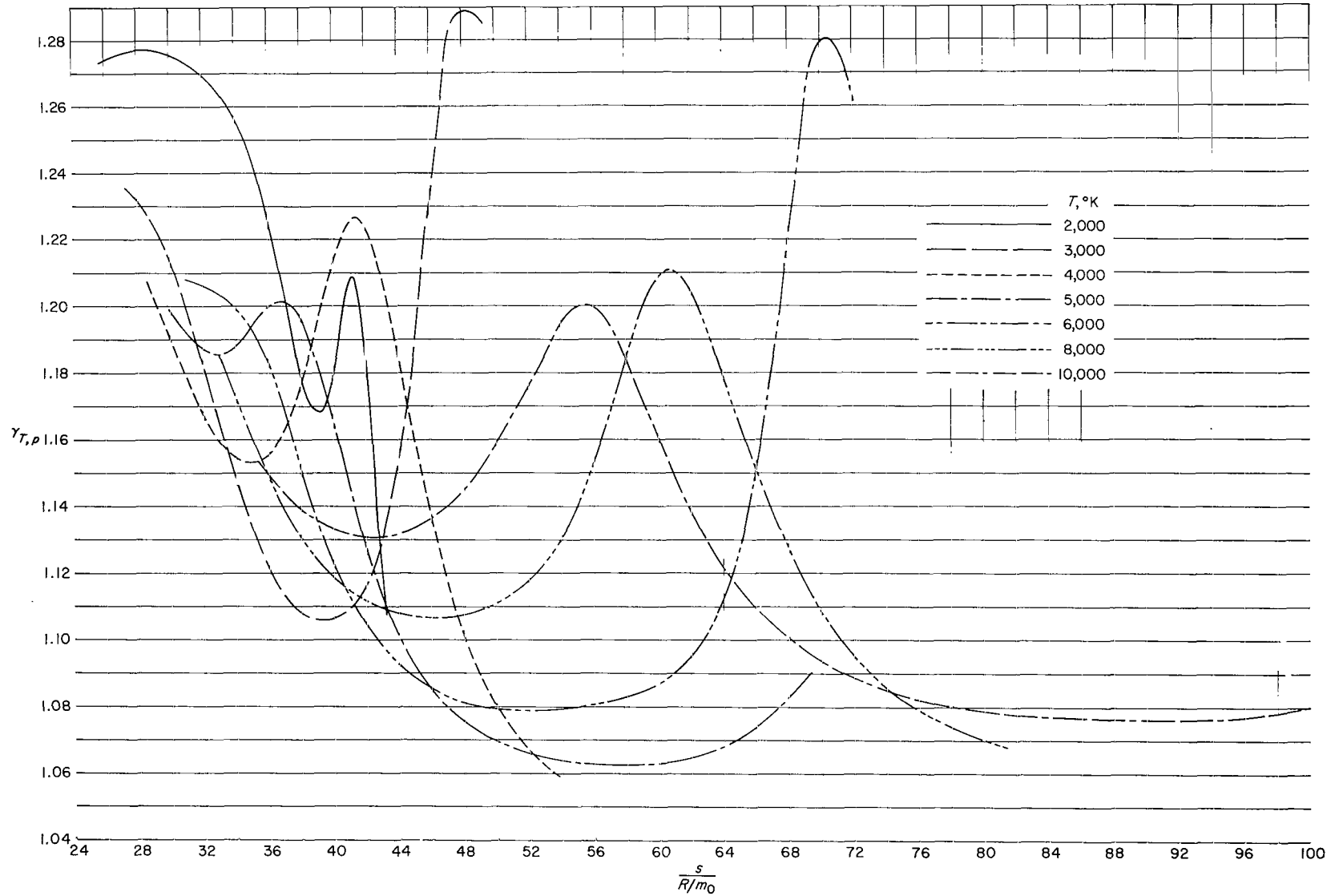
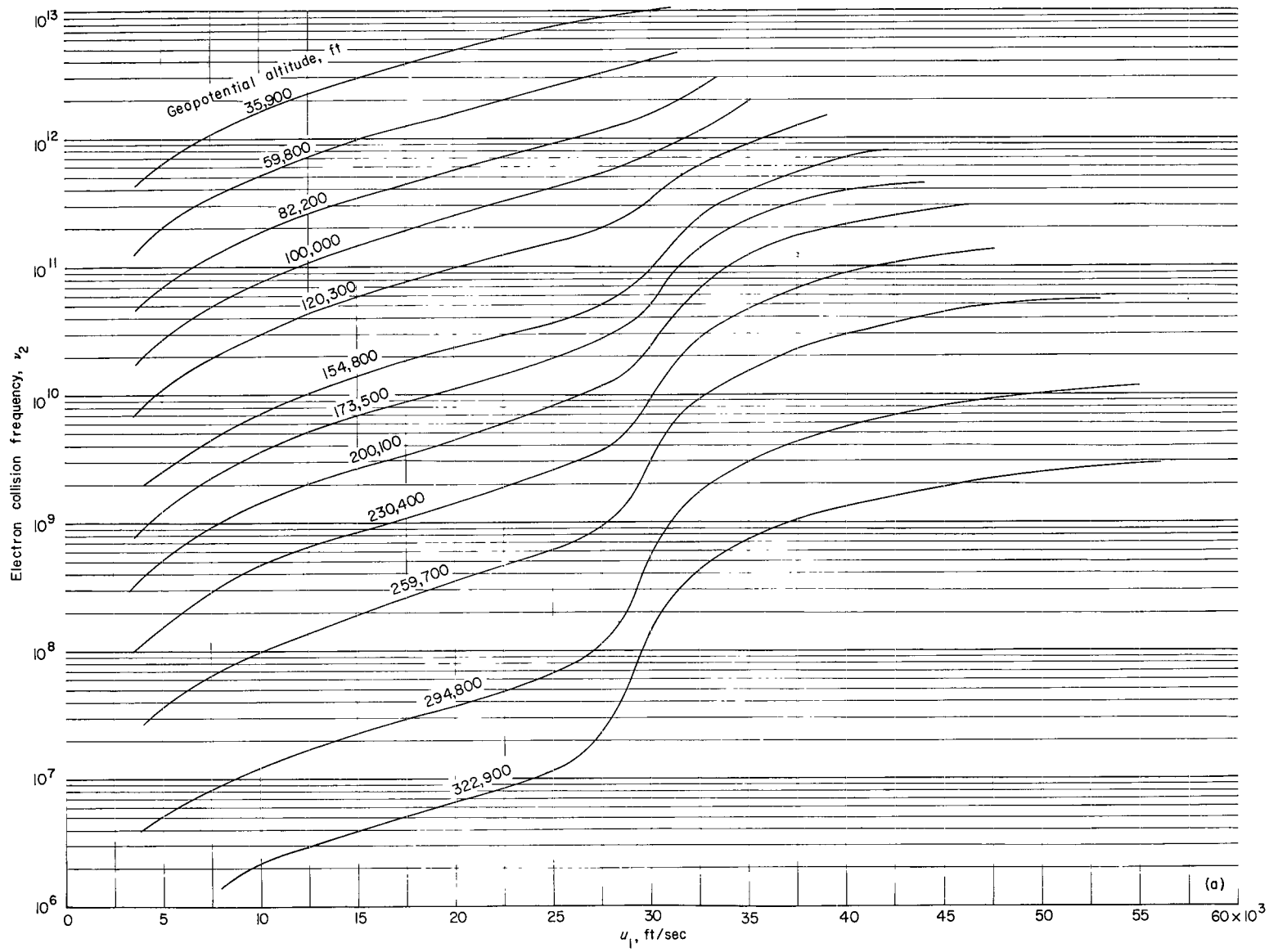
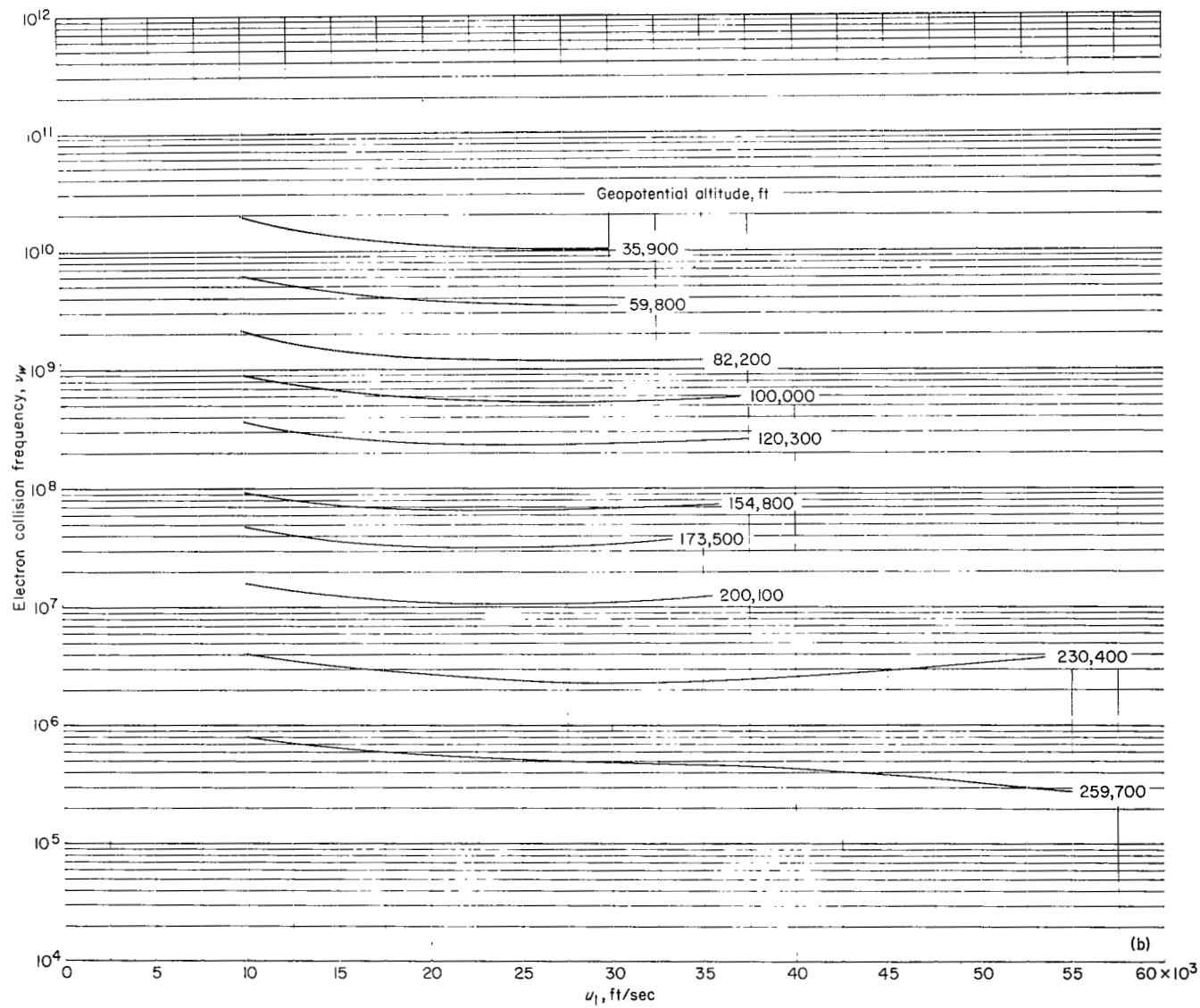


Figure 18.- Variation of the parameter $\gamma_{T,p}$ with temperature and entropy for argon-free air. (Data taken from ref. 15.)



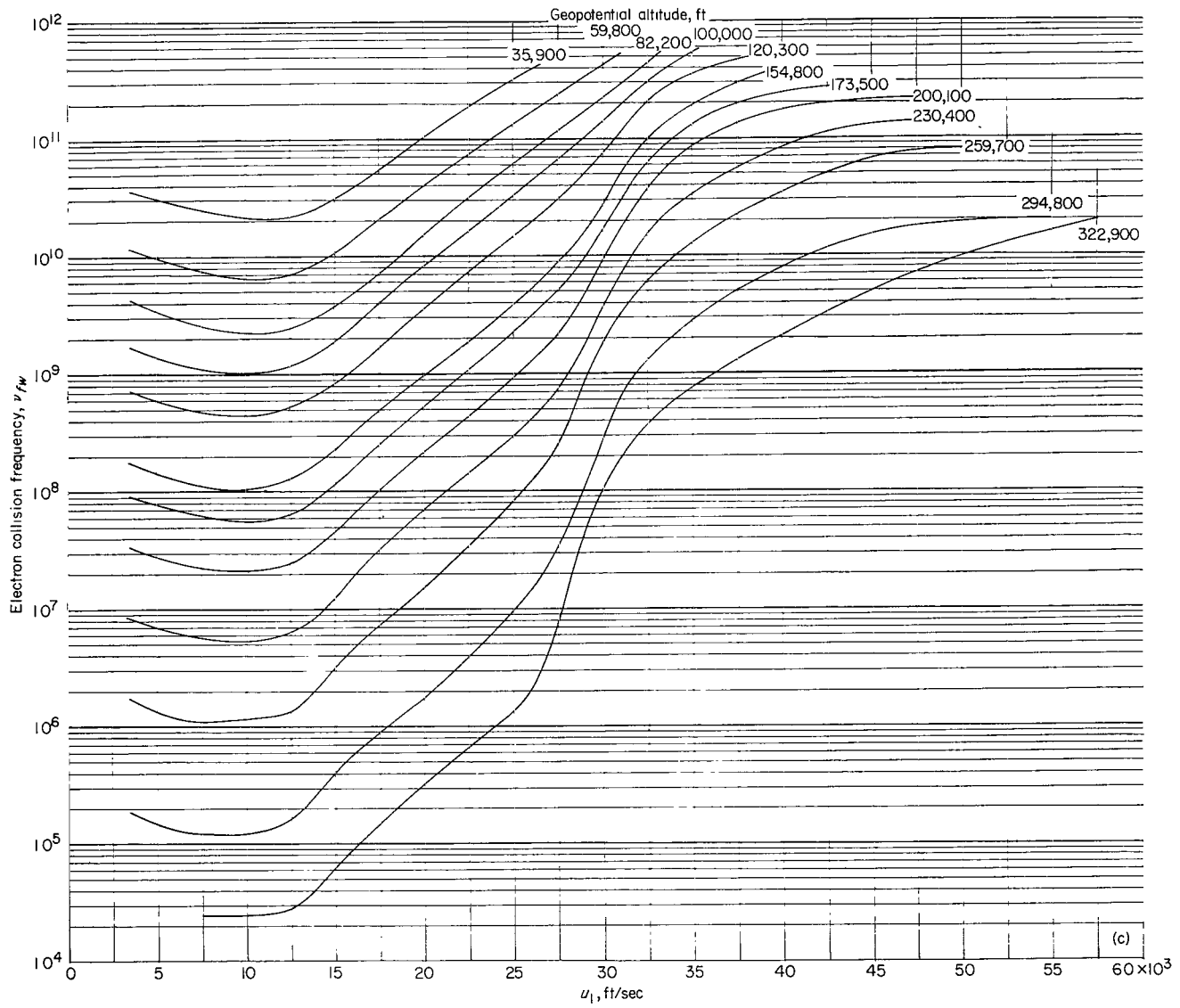
(a) Equilibrium normal-shock flow.

Figure 19.- Variation of electron collision frequency with velocity and altitude.



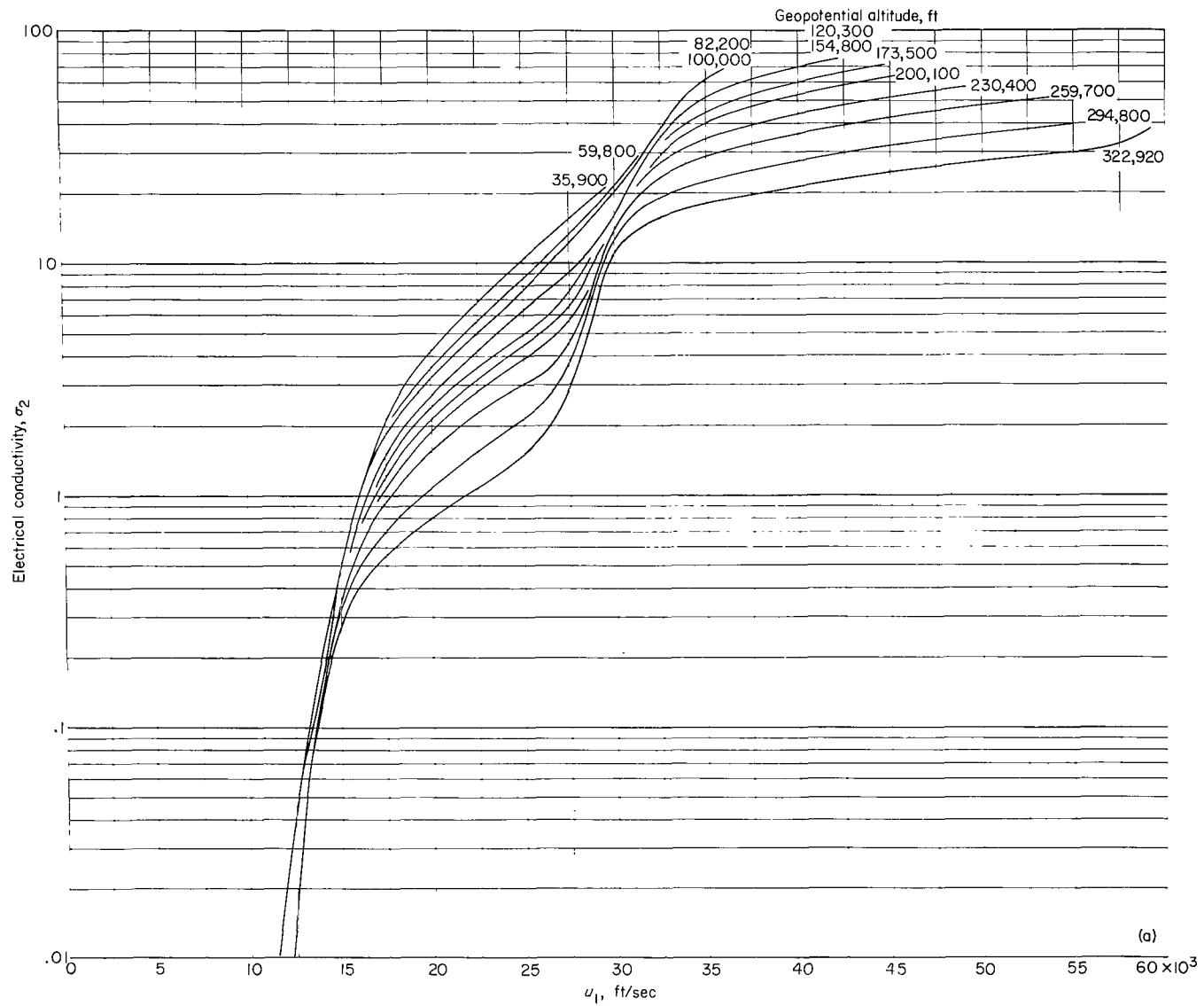
(b) Equilibrium far-wake flow.

Figure 19.- Continued.



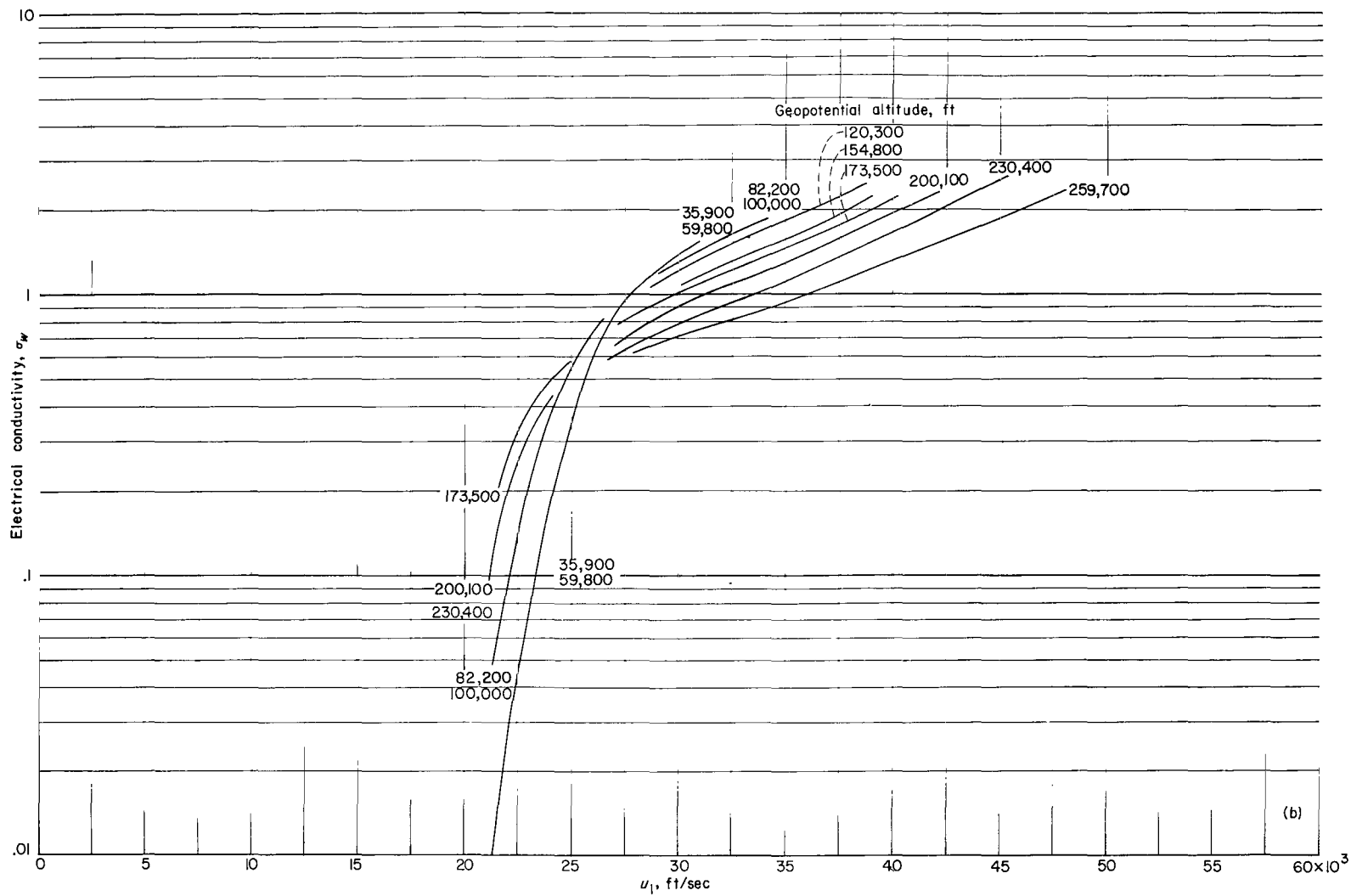
(c) frozen far-wake flow.

Figure 19.- Concluded.



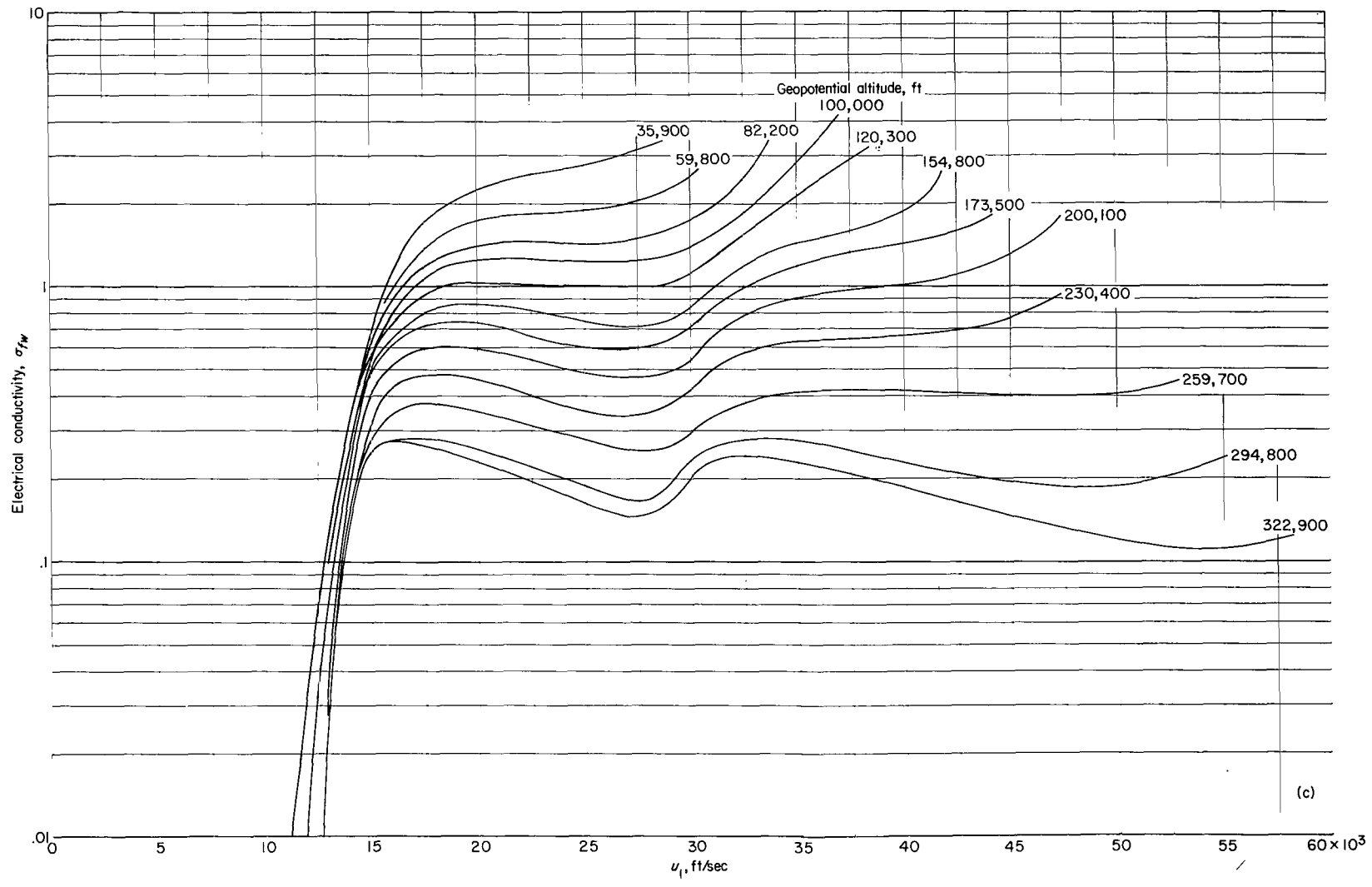
(a) Equilibrium normal-shock flow.

Figure 20.- Variation of d.c. electrical conductivity with velocity and altitude.



(b) Equilibrium far-wake flow.

Figure 20.- Continued.



(c)

(c) Frozen far-wake flow.

Figure 20.- Concluded.

"The aeronautical and space activities of the United States shall be conducted so as to contribute . . . to the expansion of human knowledge of phenomena in the atmosphere and space. The Administration shall provide for the widest practicable and appropriate dissemination of information concerning its activities and the results thereof."

—NATIONAL AERONAUTICS AND SPACE ACT OF 1958

NASA SCIENTIFIC AND TECHNICAL PUBLICATIONS

TECHNICAL REPORTS: Scientific and technical information considered important, complete, and a lasting contribution to existing knowledge.

TECHNICAL NOTES: Information less broad in scope but nevertheless of importance as a contribution to existing knowledge.

TECHNICAL MEMORANDUMS: Information receiving limited distribution because of preliminary data, security classification, or other reasons.

CONTRACTOR REPORTS: Technical information generated in connection with a NASA contract or grant and released under NASA auspices.

TECHNICAL TRANSLATIONS: Information published in a foreign language considered to merit NASA distribution in English.

TECHNICAL REPRINTS: Information derived from NASA activities and initially published in the form of journal articles.

SPECIAL PUBLICATIONS: Information derived from or of value to NASA activities but not necessarily reporting the results of individual NASA-programmed scientific efforts. Publications include conference proceedings, monographs, data compilations, handbooks, sourcebooks, and special bibliographies.

Details on the availability of these publications may be obtained from:

SCIENTIFIC AND TECHNICAL INFORMATION DIVISION
NATIONAL AERONAUTICS AND SPACE ADMINISTRATION

Washington, D.C. 20546